Remote Sensing of Environment 331 (2025) 115009

Contents lists available at ScienceDirect

Remote Sensing of Environment

journal homepage: www.elsevier.com/locate/rse

Tropical peatland hydrological dynamics affect the efficacy of C-band Small BAseline Subset InSAR approaches

Magdalena M. Mleczko [a,g,*], Kitso Kusin [b], Teuntje P. Hollaar [c], Mark E. Harrison [d,e], Nomeritae Nomeritae [f], Darmae Nasir [b], Marek S. Mróz [g], F.J. Frank van Veen [d], Muhammad A. Imron [h], A. Jonay Jovani-Sancho [i,j], Chris D. Evans [i], Adi Jaya [b,k], Karen Anderson [a]

[a] Environment and Sustainability Institute, University of Exeter, Penryn TR10 9EF, United Kingdom
[b] Centre of International Cooperation in Sustainable Management of Tropical Peatland (CIMTROP), University of Palangka Raya, Palangka Raya 73112, Indonesia
[c] Department of Earth Sciences, Faculty of Geosciences, Utrecht University, Princetonlaan 8, 3584 CB, Utrecht, the Netherlands
[d] Department of Earth and Environmental Science, Faculty of Environment, Science and Economy, University of Exeter, Penryn TR10 9EF, United Kingdom
[e] School of Geography, Geology and the Environment, University of Leicester, Leicester LE1 7RH, United Kingdom
[f] Department of Civil Engineering, University of Palangka Raya, Palangka Raya 73112, Indonesia
[g] Institute of Geodesy and Civil Engineering, University of Warmia and Mazury, Olsztyn 10-719, Poland
[h] Faculty of Forestry, Universitas Gajah Mada, Yogyakarta 55281, Indonesia
[i] United Kingdom Centre for Ecology and Hydrology, Bangor, United Kingdom
[j] School of Biosciences, University of Nottingham, Loughborough, United Kingdom
[k] Faculty of Agriculture, University of Palangka Raya, Palangka Raya, Indonesia

ARTICLE INFO

Keywords:
Tropical peatlands
SBAS
InSAR
Groundwater level
Peat surface
Soil moisture
Ground displacements
Coherence
Sentinel-1

ABSTRACT

Tropical peatlands storing ~18–25 % of global peat volume contribute significantly to the global carbon cycle. To balance preservation and protection of tropical peatlands requires assessment of their ecohydrological conditions and continuous monitoring through seasons. This is challenging to achieve using *in situ* sampling, but there is a great promise to use C-band Sentinel-1 data for this due to its weather-independence, and particularly its increased acquisition capacity and spatial/temporal resolution compared to L- and P-band current sensors. Acknowledging that Small BAseline Subset (SBAS) Interferometry using C-Band Sentinel-1 data has been shown previously to be useful for retrieving peatland surface displacement, but also that the amplitude and phase of the SAR signal are dependent on surface hydrology; there remains a critical question about the extent to which the efficacy of SBAS approaches is themselves sensitive to surface hydrological conditions. This is a particular methodological concern in tropical peatlands due to the dynamically changing hydrological conditions arising from significant rainfall events, which can cause groundwater level (GWL) to vary from 1 m to −2 m. The research area was situated in lowland Central Kalimantan (Indonesia) using Synthetic Aperture Radar (SAR) observations from the 2017–2022 period. We used SBAS-derived ground displacements and compared to groundwater level (GWL) and peat surface elevation acquired from local networks of monitoring sites. Our work shows that the prevailing hydrological condition affects the area efficacy of the SBAS approach using C-band SAR data. When surface water significantly floods above the ground surface during the wet season, the coherence is not sustained for a long time. This is the opposite of the dry season, when coherence is preserved in longer intervals between acquisitions. Additionally, the range of correlation values between SBAS-derived displacements and *in-situ* peat surface and ground water table measurements is higher for the dry season than for the wet and whole hydrological year. We show that the SBAS approach can retrieve surface displacement for 34.4 % to 59.8 % on the peat soils of the tested area (391 to 826 km2), excluding areas of dense forests and open water, due to C-band SAR limitations, *i.e.* volume scattering mechanism and/or loss of signal coherence on water bodies. We show that appropriate hydrological conditions must be met to determine the change in water level above the ground surface. Too large fluctuations in water level may not be detected because of wavelength limitations, and outliers from the assumed linear model may be filtered out or removed due to the specific properties of this

* Corresponding author: Environment and Sustainability Institute, University of Exeter, Penryn TR10 9EF, United Kingdom.
E-mail addresses: m.m.mleczko@exeter.ac.uk, magdalena.mleczko@uwm.edu.pl (M.M. Mleczko).

https://doi.org/10.1016/j.rse.2025.115009
Received 12 November 2024; Received in revised form 13 August 2025; Accepted 4 September 2025
Available online 23 September 2025

approach. These findings underpin the application of Sentinel-1C-band SAR for monitoring tropical peatlands' ecohydrological conditions.

1. Introduction

Tropical peatlands store large quantities of terrestrial carbon (469–694 Giga tons of C (Page et al., 2011; Ribeiro et al., 2021)) and deliver numerous important ecosystem services to humans, whilst also supporting conservation of species and habitats of international importance (Posa et al., 2011). In dry years, widespread wildfires in tropical peatlands can burn for months with huge impacts locally, regionally and globally (Liu et al., 2017). These major fire events are strongly linked to the droughts caused by El Niño Southern Oscillation (ENSO) climate events (Putra, 2011; Sze and Jefferson Lee, 2019). This is particularly concerning because such El Niño events are predicted to increase in frequency under global warming and ongoing deforestation (Cai et al., 2014; Davies-Barnard et al., 2023; Thirumalai et al., 2017), and there has been a coupled trend of reduced rainfall over recent decades (McAlpine et al., 2018). Among other needs, preservation and protection of valuable peatland areas requires assessment and continuous monitoring of the hydrological condition of the peatlands. Yet both ground- and remote-based peatland monitoring is challenging, particularly in tropical areas because the peat surface itself may be overlain by a wide variety of land cover types from dense forest to more anthropogenic ones (*e.g.* agriculture; (Page et al., 2011)).

The key characteristics of undisturbed tropical peatlands include high vegetation species richness, and high water tables (Page et al., 2009). Monitoring of tropical peatlands from remote sensing follows different methods, predominantly passive optical and active Synthetic Aperture Radar (SAR) approaches (Minasny et al., 2019). SAR has been found to be a particularly useful technique for tropical peatland monitoring because it offers a weather-independent technique and is suited to act in wet climates where cloud cover degrades capability of effective optical acquisitions (Tanase et al., 2020; Waqar et al., 2020; Widodo et al., 2019). Furthermore, strong development of SAR systems has been noted in recent years, especially with the launch of the ESA's Sentinel-1 (S1) satellites – opening a new chapter of SAR mapping by delivering free, almost unlimited access to C-band SAR images. Key advantages of S1 are the wide swath (250 km) and 12-day revisit cycle in case of one operating satellite or 6-days with two satellites operating (noting recent loss of Sentinel 1b due to a power supply issue in December 2021; with subsequent replacement Sentinel 1c launched in December 2024 and at the time of writing undergoing operational commissioning). Increased accessibility not only to SAR data but also to open source solutions that leverage free to use data are especially important for less economically-resourced countries such as Indonesia, which contains 36 % of the world's tropical peatlands, much of which is relatively inaccessible (peatland land cover accounts for approximately 7.8 % of Indonesia's extent (World Bank Group, 2018). Its sensitivity to soil moisture and roughness leads to SAR having a great potential role for monitoring the hydrological conditions of tropical peatlands, although this has yet to be deeply explored. SAR approaches are widely used in hydrological studies; including i) water bodies detection and delineation of their extent, including evaluation and monitoring of open surface water (Dellepiane and Angiati, 2012; Matgen et al., 2011; Pulvirenti et al., 2016) and water in emergent vegetation (Brisco et al., 2019; Grimaldi et al., 2020; Mleczko et al., 2021; Plank et al., 2017; Tsyganskaya et al., 2018) ii) soil moisture (SM) estimation (Barrett et al., 2009; Dabrowska-Zielinska et al., 2018; Kim et al., 2017; Lopez-Sanchez et al., 2021; Ranjbar et al., 2021), iii) estimation of changes in water level above the ground (Gondwe et al., 2010; Hong et al., 2022; Hong and Wdowinski, 2014; Liao et al., 2020), iv) estimation of changes in groundwater levels (GWL) (Asmuß et al., 2019; Bechtold et al., 2018; Khakim et al., 2020; Tampuu et al., 2020b; Zhou et al., 2019). A broad range of SAR techniques are used for these tasks, from backscattering intensity analyses, through polarimetry (PolSAR) to Differential SAR Interferometry (DInSAR).

DInSAR (*e.g.* PSI – Persistent Scatterer Interferometry, SBAS – Small BAseline Subset Interferometry) is considered as a reliable tool for mapping of motions and deformations of the ground/ land. Various drivers of surface movements: tectonics, engineering works, mining activity / post mining ground motion, water pumping, gas exploration, and relevant to this piece: "bog breathing" (Tampuu et al., 2023), which is the vertical deformation of peatland surfaces in response to water table changes. InSAR PSI has some limitations in monitoring surface deformation, *e.g.* due to lack of strong scatterers / permanent scatterers (PS), also called MP (measurement points) and/or low temporal coherence of the complex signals. SBAS based on distributed scatterers also has similar limitations due to low coherence in densely vegetated areas. Coherence (interferometric correlation) is a crucial parameter for successful or unsuccessful phase difference measurements. Coherence variability on wetlands, peatlands and generally grasslands, on the other hand, is strongly related to hydrological conditions determining scattering mechanisms: advantageous or disadvantageous with further consequences in InSAR products usability/ applicability (Scott et al., 2017).

DInSAR approaches have been shown to have high sensitivity to surface swelling or subsidence with sub-centimetre precision (Hanssen, 2001), and therefore the potential ability to hydrological monitoring *via* the estimation of changes in GWL (Evans et al., 2021; Wösten et al., 1997). Basis of DInSAR is the microwave phase difference measurement along with correlation of the complex SAR signal over time (between two or more consecutive acquisitions). Tropical peatlands being mixed and composite vegetated areas give temporally irregular coherent measurements, thus the key element in the proposed approach is to choose a solution that can deal with the temporal decorrelation or minimise its impact. Such a method is offered by the SBAS approach which leverages sequential SAR acquisitions mitigating spatial and temporal decorrelation effects of so-called distributed targets'. So far, dedicated tropical peatland studies using InSAR long-time series have been scarce and encompassed the L-band (Hoyt et al., 2020; Umarhadi et al., 2022; Zhou et al., 2019), with studies exploring C-band (Izumi et al., 2022a, 2022b; Khakim et al., 2020; Marshall et al., 2018; Zheng et al., 2023a) or multifrequency combination of C- and L-band (Umarhadi et al., 2021). The studies have shown that longer wavelength SAR data (*e.g.* L- and P-band) are considered more appropriate for interferometric SAR analysis of complex natural environments, due to penetration ability through vegetation canopy. Whilst C-band shows strong potential for measuring peatland surface motion, because of its fine spatial resolution and improved temporal resolution given the multiple current and upcoming SAR platforms with C-band instruments onboard (Torres et al., 2017). The usefulness of C-band data and the feasibility of the SBAS approach for monitoring long-term surface motion has been tested with ERS and Sentinel-1 images over peatland in the northeast of Scotland (Alshammari et al., 2018), which despite having a very different climate, exhibits similar morphology to tropical peatlands (albeit with less complex overlying vegetation cover compared to tropical systems). Sentinel-1 data have also been used to evaluate whether "bog breathing" can be measured by multitemporal DInSAR in Northern temperate raised bogs in Estonia (Tampuu et al., 2022). Although the authors (*ibid.*) questioned the accuracy of the approach over peatlands due to underestimation of real surface displacements and despite a serious phase unwrapping problem, a potential for assessment of short-term peatland surface displacements in favourable conditions using time series was stated. Recent efforts to estimate tropical peatland

subsidence using C-band Sentinel-1 data and correlate results with GWL were made by Izumi et al., 2022b showing a developed approach based on SBAS to increase the density of coherent scatterers for tropical peatland deformation monitoring. On the other hand, DInSAR measurements are sensitive to both: i) topographic displacements and ii) changes in soil moisture (Zwieback et al., 2017) and these can affect interferometric phase in ways that are challenging to uncouple. There are several studies addressing the relationship between interferometric observables and soil moisture (de Zan et al., 2014; Hrysiewicz et al., 2023; Molan and Lu, 2020; Ranjbar et al., 2021; Zwieback et al., 2017), showing that L-band InSAR phases are highly correlated to soil moisture and more sensitive compared to coherence and phase triplet (Molan and Lu, 2020). The studies concerning shorter wavelength (C-band) show that the linear regression model can accurately estimate soil moisture over bare soils for short temporal baselines, where deformation and other changes depending on the temporal baseline are negligible (Ranjbar et al., 2021), but vegetation interferes with the signal and introduces uncertainties.

Acknowledging that SBAS Interferometry using C-Band Sentinel-1 data has been shown previously to be useful for retrieving peatland surface displacement (Hrysiewicz et al., 2024; Hrysiewicz et al., 2023; Tampuu et al., 2023; Tampuu et al., 2022; Tampuu et al., 2020b), but also that the amplitude and phase of the SAR signal are dependent on surface hydrology, there remains a critical question about the extent to which the efficacy of SBAS approaches is themselves sensitive to surface hydrological conditions. Some studies refer to the link between InSAR-derived displacements, soil moisture and groundwater level (Hrysiewicz et al., 2023). Marshall et al. (2022) indicate that drought events can potentially lead to unreliable estimates of high subsidence rates. These findings are primarily based on temperate peatlands, which typically exhibit lower variability in groundwater level (GWL) changes. In temperate regions, GWL fluctuations generally range from 0.2 m to −0.3 m (Hrysiewicz et al., 2023; Tampuu et al., 2020a), whereas in tropical peatlands, GWL can vary more dramatically, from 1 m to −2 m. While the fundamental limitations of InSAR on peatlands — such as coherence loss, phase ambiguity, and temporal decorrelation — are common to both climatic zones, tropical peatlands tend to exhibit lower overall coherence. This can be largely due to their dynamic hydrological conditions, influenced by frequent and intense rainfall events (Hoyt et al., 2024). Consequently, interpreting InSAR-derived subsidence in tropical peatlands presents particular methodological challenges that require careful consideration. Segmenting the analysis according to hydrological years (November – October) and using a test site in Central Kalimantan (Indonesia) exhibiting diverse land cover, we investigate the following questions across the 2017–2022 period and compare to groundwater levels from SIPALAGA (https://sipalaga.brg.go.id/https://sipalaga.brg.go.id/), soil moisture from SEPAL project (https://sepal.io/) and peat camera system data showing surface elevation and groundwater levels from Evans et al. (2021). We tackled two following questions:

– Does the area-effectiveness and reproducibility of the SBAS approach on an inter-annual basis depend on hydrological conditions and if so, how?

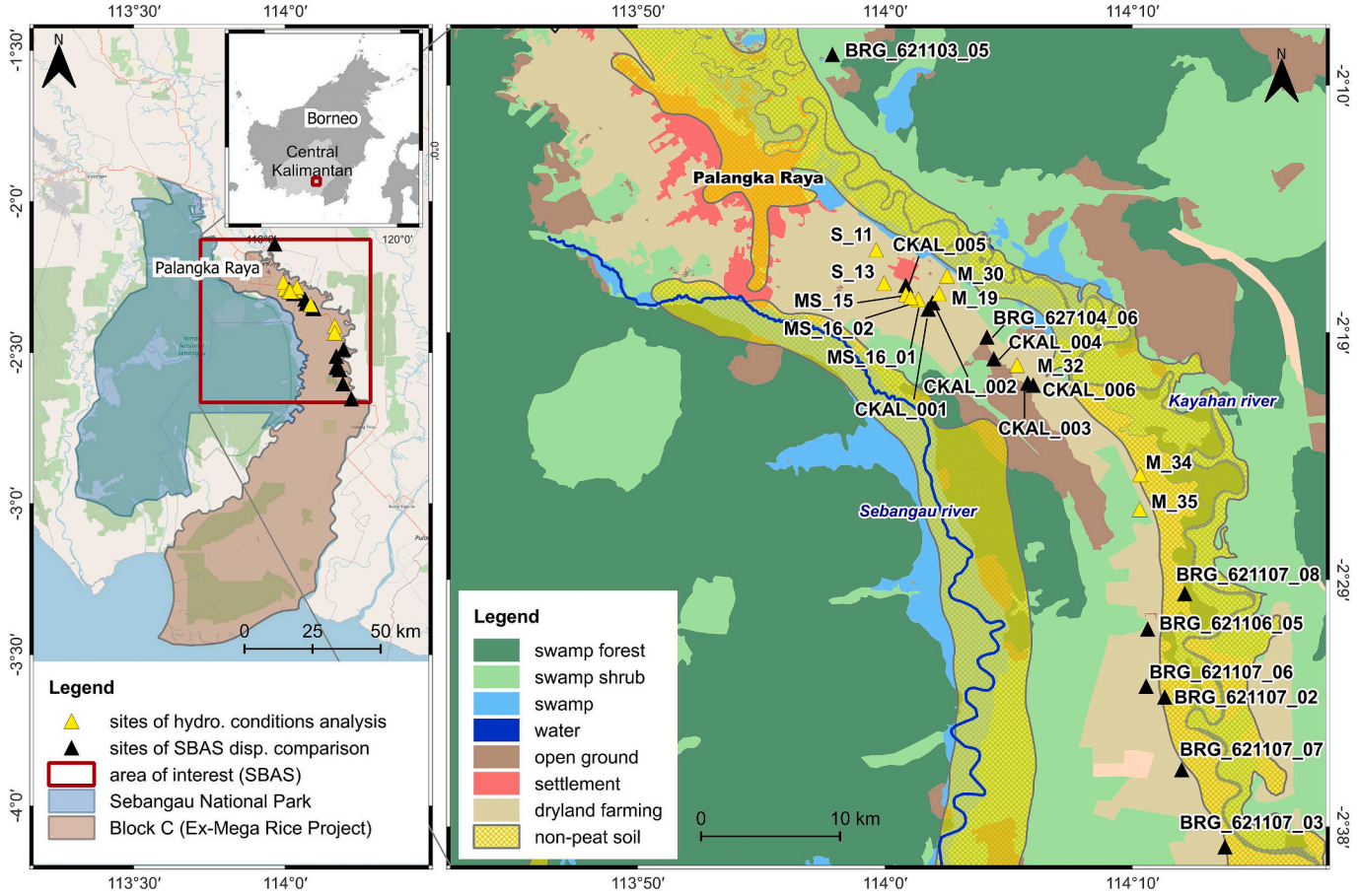

Fig. 1. Location of the study area, Central Kalimantan in Indonesia (left map). Land cover map of the study area for 2019 provided by the Ministry of Environment and Forestry Indonesia (right map) with an overlaid area of non-peat soils. The locations of sites used to evaluate the correspondence between *in situ* observations of peat surface and GWL and time series of displacements are represented by black triangles, sites for evaluating how surface hydrological conditions impact time series of coherence are highlighted by yellow triangles. (For interpretation of the references to colour in this figure legend, the reader is referred to the web version of this article.)

– How does the correspondence between SBAS-derived displacement and *in situ* observations (ground water level and surface elevation) vary with hydrological conditions?

2. Study area and datasets

2.1. Description of the area of interest (AOI)

The specific area of interest (3750 km^2) is located in the lowlands of Central Kalimantan (Indonesian Borneo) in a region to the southeast of Palangka Raya city (Fig. 1). An official land cover map provided annually by the Ministry of Environment and Forestry Indonesia (Indonesian: Kementerian Lingkungan Hidup dan Kehutanan – KLHK) is shown in Fig. 1 (right inset). Fig. 1 shows land cover product from 2019, while Fig. S1 in supplementary materials provide annual land cover maps covering all analysed years 2017–2022. The overall percentage distribution of land use/land cover classes for the AOI is: swamp forest 47 %, swamp shrubs 26 %, farmland 14 %, bare land 5 %, wetland 4,5 %, urban area 2 %, water bodies 1,5 % (KLHK, 2022). The area around Palangka Raya is comprised of tropical land covers of varying types (from agricultural to intact primary peat swamp forest) underlain by peat of varying depths between 1 and 10 m (Hayasaka et al., 2020; Widyatmanti et al., 2022). Fluvisols are found around the rivers (the generalised location on Fig. 1 is from a map scale 1:50000; (KLHK, 2022)). Some parts of this region were heavily deforested and drained for the Indonesian Mega Rice Project (MRP) (Page et al., 2009), and since then parts of the region have been affected by severe and repeated fires (Hoscilo et al., 2011). Our research area incorporated the so-called Block C of the ex-MRP, which contains the peat dome between the Sebangau and Kahayan rivers. Block-C is composed of heterogeneous mixtures comprising patches of secondary forest fragments, smallholder agriculture, oil palm plantations, and regions of degraded shrubland dominated by ferns, regenerating native trees and non-native *Acacia mangium* (Page et al., 2009). There is a zone bordering the Kayahan river labelled in the land cover map (Fig.1 right inset map) as a relatively large homogenous class of 'dryland agriculture' - in reality this classification belies the true heterogeneity of what is very diverse ecology on the ground (see later detailed site descriptions for sites M32, M34, M35 which lie in this region). To the west of the degraded Block C study area, lies the Sebangau National Park, a much less impacted protected area with relatively undisturbed tropical forest, which has been less affected by fires (Atwood et al., 2016). Both regions (Sebangau National Park and Block C) were part of our study region and DInSAR calculations. The AOI is considered geologically stable, so no ground motion could be attributed to tectonics. There is no ongoing underground work that could cause ground surface displacements. According to (Wösten et al., 2008), oxidation accounts for 60 % of peat subsidence on average, with irreversible drying or shrinking of peat accounting for 40 %.

2.2. Sites of interest for specific analyses

The whole AOI and additional test sites chosen within AOI for detailed analysis (yellow triangles in Fig.1) are used here to answer the research questions. Initially, we identified 40 test sites using the SAR data, with site choice based on attributes of high InSAR coherence and varying topographic dynamics, and accessibility for ground verification (*i.e.* proximity to roads or canals). Following consultation with Indonesian authorities and team members with experience in these areas on the ground, the list of sites was reduced to ten feasible areas where detailed *in situ* analyses could be undertaken for validation purposes (Table 1 and Fig. 2). The remaining 30 sites were unfeasible due to local conflict, ongoing activities at the site which precluded access, or inability to contact the landowner. The ten selected sites represent a broad spectrum of peat depth ranging from 0.5 to 8 m and are classified as agricultural fields or swamp shrubland (KLHK, 2022). In all cases, the sites labelled as having agricultural land cover were not subject to

Table 1
Characteristics and management histories of test sites used to answer the question of how surface hydrological conditions affect SBAS-derived results.

Test site	Land use (based on KLHK database)	Peat depth [m] (based on *in situ* observations)	Vegetation (based on *in situ* observations)	Fire history (based on MODIS fire product)
S_11	agricultural field (uncultivated)	0.6	*Acacia auriculiformis A. Cunn. ex. Benth.; Scirpus juncoides Roxb.; Melastoma malabathricum L.;*	2019
S_13	agricultural field (uncultivated)	1.2	*Acacia auriculiformis A. Cunn. ex. Benth.; Melastoma malabathricum L.; Cratoxylon glaucum Korth.; Scirpus juncoides Roxb.*	2019
MS_15	agricultural field (uncultivated, lying tree trunks)	2.2	*Acacia auriculiformis A. Cunn. ex. Benth.; Cratoxylon glaucum Korth.; Ploiarium elegans Korth.; Melastoma malabathricum L.*	2009, 2014, 2019
MS_16_01	agricultural field (uncultivated, lying tree trunks)	2.4	*Acacia auriculiformis A. Cunn. ex. Benth.; Melastoma malabathricum L.; Cratoxylon glaucum Korth.; Ploiarium elegans Korth.*	2014, 2019
MS_16_02	agricultural field (uncultivated)	2.5	*Stenochlaena palustris, Dicranopteris linearis, Melastoma malabathricum, Acacia sp., Cratoxylon glaucum, Baeckea frutescens, Ploiarium alternifolium*	2014
M_19	agricultural field (uncultivated)	3.6	*Acacia auriculiformis A. Cunn. ex. Benth*	2002, 2014
M_30	agricultural field (inundated most of the time)	0.5	*Lepironia articulata, Blechnum indicum, Acacia sp., Melaleuca leucadendra*	2003, 2009, 2014, 2019
M_32	swamp shrubland	2.0	*Blechnum indicum, Stenochlaena palustris, Baeckea frutescens, Acacia sp., Combretocarpus rotundatus, Ploiarium alternifolium*	2004, 2009, 2014, 2019
M_34	swamp shrubland	7.0	*Blechnum indicum, Elaeis guineensis, Syzygium sp., Melaleuca leucadendra, Combretocarpus rotundatus*	2014
M_35	swamp shrubland	8.0	*Nephrolepis biserrate, Lepironia articulata, Melaleuca*	2015

(*continued on next page*)

Table 1 (*continued*)

Test site	Land use (based on KLHK database)	Peat depth [m] (based on *in situ* observations)	Vegetation (based on *in situ* observations)	Fire history (based on MODIS fire product)
			leucadendra, Cratoxylon glaucum, Acacia sp., Combretocarpus rotundatus, Baeckea frutescens	

agrarian treatments. All test sites suffered wildfire impacts at some point in the past, and for six test sites (one swamp shrubland M_32 and five agriculture fields S_11, S_13, MS_15, MS_16_01, and M_30) active fires burned the sites during the analysed period in the year 2019 (Table 1). One uncultivated agricultural field test site (M_19) was subjected to removal of woody vegetation. At four test sites (S_11, M_19, M_30, M_32), water above the ground was detected based on visual inspection of optical satellite data, *i.e.* Planet, Sentinel-2, Landsat and field reconnaissance.

To answer the second question about the correspondence between SBAS-derived displacement and *in situ* observations (ground water level and surface elevation) varying with hydrological conditions we used the group of test sites shown in Table 2.

The availability of adequate *in situ* observations describing hydrological conditions (SM – soil moisture, GWL – groundwater level) for validation of the satellite products over a multi-year period is very challenging in this situation due to the heterogeneous land cover across the study area, which ranges from a dense forest in Sebangau National Park to more open, heavily managed land covers in Block C. In the region, there are some measurement stations managed by the Indonesian Peat and Mangrove Restoration Agency (BRGM) providing real-time (hourly temporal resolution) groundwater level (m) and soil moisture (kg/m2) data. Daily data are available freely from the "Sistem Pemantauan Air Lahan Gambut" (SIPALAGA) project (https://sipalaga.brg.go.id/). For each variable, minimum, mean, and maximum values are provided for each measurement date. In this study, we obtained data from the eight SIPALAGA stations that sit within our AOI, at daily intervals in the periods specified in Table 2. Additionally, we gathered data from six measurement stations of the novel low-cost and high-resolution camera system developed as a part of the project PASSES: Peatland Assessment in Southeast Asia by Satellite, and project SUSTAINPEAT: Overcoming barriers to sustainable livelihoods and environments in smallholder agricultural systems on tropical peatland (Evans et al., 2021). Peat cameras provided measurements of peat surface subsidence and water table dynamics in periods specified in Table 2. We used GWL and peat surface displacement to compare them with displacements measured from SBAS (question 2) at SIPALAGA and PASSES peat cameras locations (Fig. 1 and Table 2).

Over all test sites, we obtained information about SM from the soil moisture content maps of the System for Earth Observation Data Access, Processing and Analysis for Land Monitoring (SEPAL; https://sepal.io/). SEPAL is an open-source platform that provides sufficient spatial resolution (< 50 m) and timing to check how SM affects SBAS results. SM from SEPAL is estimated based on multispectral (Sentinel-2, Landsat-8) images and SAR data (Sentinel-1) and validated using ground-based SIPALAGA measurements, with an overall estimation accuracy of Root-Mean-Squared-Error (RMSE) 0.04 m^3m^{-3} and R^2 0.81 (Greifeneder et al., 2021). It is worth noting that SM from SEPAL shows only relative values, while ground measurements show absolute SM values, which results in SM differences between the two sources.

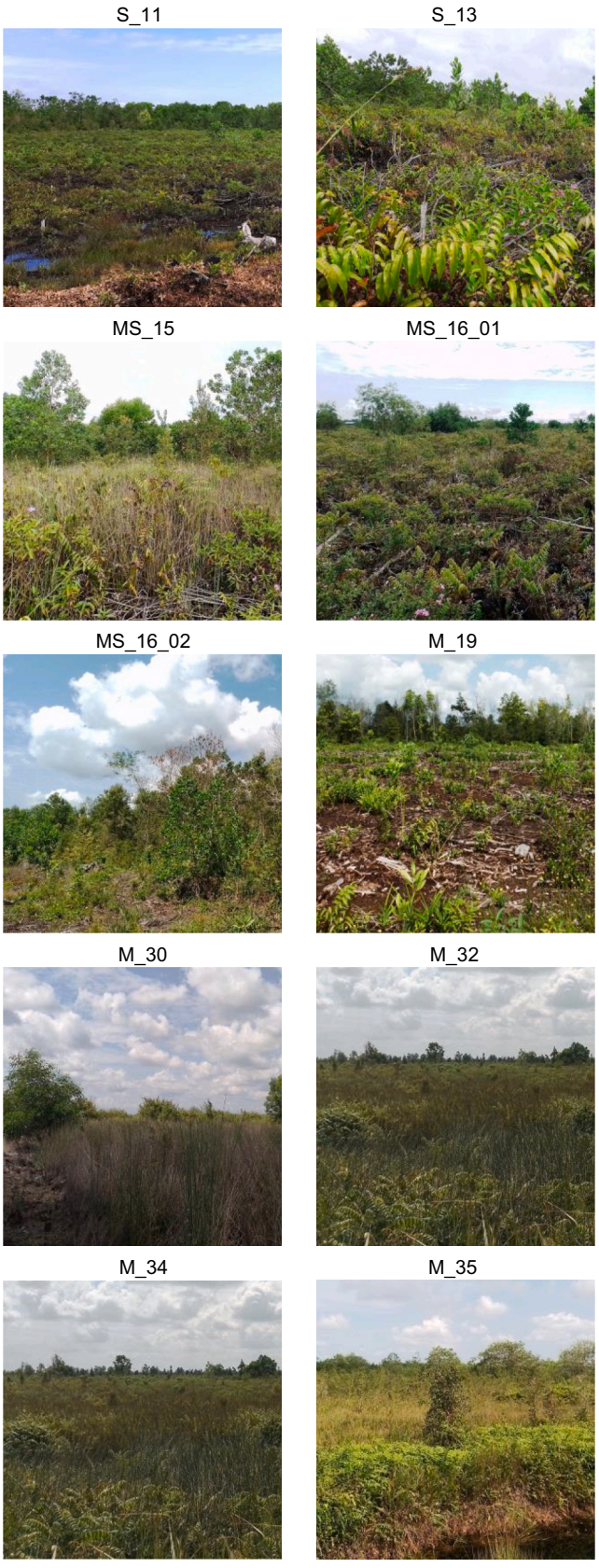

Fig. 2. Representative pictures of the test sites used for evaluating how surface hydrological conditions impact time series of coherence.

Table 2
Characteristics of sites used to compare *in situ* measurements (GWL and surface elevation) with SBAS-derived displacements.

Test site	Land use (based on KLHK database 2019)	Peat depth [m]	*In situ* data type*	Data availability time
BRG_621103_05	swamp shrubland	1.5	GWL, SM	02/12/2018–17/04/2020, 19/04/2022–31/10/2022
BRG_621106_05	agricultural field	5.5	GWL, SM	19/04/2022–31/10/2022
BRG_621107_02	agricultural field	0.0	GWL, SM	19/04/2022–31/10/2022
BRG_621107_03	agricultural field	0.5	GWL, SM	03/12/2018–17/04/2020, 19/04/2022–31/10/2022
BRG_621107_06	agricultural field	0.5	GWL, SM	19/04/2022–31/10/2022
BRG_621107_07	agricultural field	3.5	GWL, SM	19/04/2022–31/10/2022
BRG_621107_08	agricultural field	1.0	GWL, SM	19/04/2022–31/10/2022
BRG_627104_06	agricultural field	1.5	GWL, SM	07/12/2018–17/04/2020, 19/04/2022–31/10/2022
CKAL_001	agricultural field	2.9	GWL, PS	18/01/2019–12/09/2020, 01/11/2019–12/09/2020
CKAL_002	agricultural field, oil palm	3.8	GWL, PS	22/12/2018–19/10/2021, 21/01/2011–28/10/2022
CKAL_003	classified as agricultural field, covered by trees	2.5	GWL, PS	24/02/2020–18/09/2020, 01/11/2019–18/09/2020
CKAL_004	open ground	2.7	GWL, PS	01/01/2019–19/09/2020
CKAL_005	agricultural field	3.6	GWL, PS	24/02/2020–19/07/2020, 01/11/2019–19/07/2020
CKAL_006	classified as agricultural fields, covered by fern shrubs	2.7	GWL, PS	27/12/2018–27/05/2020

* GWL – ground water table, SM – soil moisture, PS – peat surface elevation.

2.3. Climatic data

The climate of the test site is tropical, with a fairly distinct division into two seasons. The wet monsoonal season occurs between November and April, and a relatively drier season occurs for the rest of the year. There is some inter-annual variation in the start date of the wet and dry seasons. This is primarily caused by the influence of the El Niño Southern Oscillation (ENSO), where drier conditions are experienced during El Niño events and wetter conditions during La Niña events (World Bank Group and Asian Development Bank, 2021). Data availability for our research spanned a 6-year period (2017–2022), including both dry (El Niño) and wet years (La Niña). We term *a hydrological year* to mean the period of twelve months commencing 1 November of any given year and ending 30 October of the following year; for example, the 2013 hydrological year starts in November 2012 and ends in October 2013. The average annual rainfall for the hydrological years 2013–2022 averages at 2965 mm (Fig. 3). In the hydrological year 2019 an El Niño prevailed (https://ggweather.com/enso/oni.htm) and rainfall decreased to below 2500 mm, and very low precipitation was recorded in the dry season (below 500 mm). Rainfall was around the average in the hydrological years of 2017, 2018 and 2020, slightly below average in 2021, and 2022 was a wetter year with rainfall higher than the annual average. (Fig. 3).

2.4. Satellite data

C-band (~5.3 cm) Synthetic Aperture Radar (SAR) data acquired by the only one of the Sentinel-1 satellite of the European Space Agency (ESA) were used (only Sentinel-1 A satellite was operating over the study area at the time of analysis). A total of 159 Single Look Complex (SLC) images in Interferometric Wide (IW) swath mode from descending orbit (relative orbit 3) were used, covering the period from November 2016 to October 2022 (Table S1 in supplementary materials). The revisit time of Sentinel-1 A observations from identical observation geometry is 12

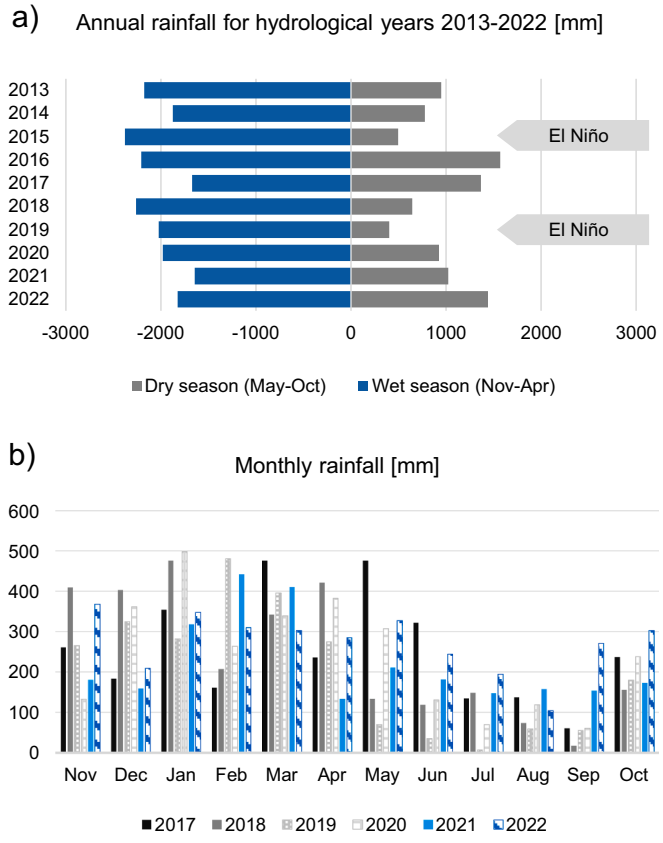

Fig. 3. a) Annual rainfall for hydrological years 2012–2022 b) Monthly rainfall for hydrological years 2017–2022 at Tjilik Riwut Meteorological Station obtained from Meteorology, Climatology, and Geophysical Agency of Indonesia (https://dataonline.bmkg.go.id/).

days. Due to technical issues like a SAR antenna anomaly, calibrations, and others reported on ESA's website [https://sentinel.esa.int/web/sentinel/news], the gaps of continuity in image acquisition of maximum 3 consecutive images were noticed a few times during the whole period. The gaps occurred in years 2019–2021 during dry season (May–July), in 2022 at the beginning of the wet season (October–November). Within the swath, the incidence angle ranged from 30° to 53°. The incidence angle to the test site varied between 32° to 36°. All scenes used included both VV and VH polarisations, but VH cross-polarised SAR images are known to be affected by volume scattering and are not preferred for interferometric applications. For this reason, only VV co-polarised images were applied to our study. The pixel spacing for gathered acquisitions is 2.32 m in the range direction and 14.05 m in the azimuth direction.

The Copernicus DEM GLO-30 was used as a reference Digital Elevation Model (DEM) in the interferometric processing. The Copernicus DEM is one of the global DSMs (Digital Surface Model) and is freely available. GLO-30 offers global coverage at a resolution of 30 m with absolute vertical accuracy less than 4 m, and absolute horizontal accuracy below 6 m (ESA, 2019).

3. Methodology

3.1. Conceptual experimental design and defining principles

Multitemporal DInSAR methods work efficiently in monitoring the temporal evolution of subtle surface deformations affecting distributed targets, but some limitations still exist (Li et al., 2022a). The essential condition for using DInSAR and achieving reliable measurements of ground displacements is to preserve phase coherence between two time-lapse SAR images (Hanssen, 2001). In our research, we have chosen the SBAS approach (Berardino et al., 2002), which uses SAR image pairs with small temporal separation to limit the effects of distributed targets' spatial and temporal decorrelation and cope with other decorrelation sources (caused by various factors, including the difference in the geometry between the two acquisitions, differences in the Doppler centroids, characteristics of the system, the specific processing parameters, the chosen algorithms and/or decorrelation caused by atmospheric heterogeneities and orbital errors (Hanssen, 2001)). We decided to use the fundamental version of SBAS (Berardino et al., 2002) as it is the principle of all modified approaches based on small baseline separation. In the literature, other methods, developed for peat surface motions and based on classical SBAS (*e.g.* ISBAS (Sowter et al., 2013); and Adaptive HCTSs SBAS-InSAR (Zheng et al., 2023b)) can also be found.

Our approach was intended to examine the factors influencing the effectiveness (area and accuracy) of the fundamental SBAS method for characterising the condition of tropical peatlands and to answer questions about the role of surface hydrological conditions in this. Fig. 4 shows the conceptual approach to the two research questions.

The first research question was answered by analysing the inter-annual multitemporal coherence and velocity maps over the whole AOI. Multitemporal coherence was estimated for each pixel, evaluating the interferometric correlation among the various stack interferograms along the temporal sequence. We also analysed how surface hydrological conditions affect phase coherence, using soil moisture from SEPAL and surface characteristic changes over ten test sites.

The second research question demanded an analysis of the correspondences between time-series of displacements measured by SBAS and *in situ* observations recorded by SIPALAGA (GWL) and PASSES (GWL and peat surface height) observations. But first, the fitting quality of the displacement model, calculated as RMSE using formula:

$$RMSE = \sqrt{\frac{1}{n}\sum_{i=1}^{n}(P_i - O_i)^2}$$

where P_i are values predicted by a linear model and O_i the values observed (derived from the displacement time series) were evaluated to determine the correspondence between satellite-derived phase measurements and displacements modelled by SBAS. Then, Pearson's correlation coefficients (r) were calculated to evaluate similarity over time with regard to the periodicity of the peat-surface motion oscillations, which aligns with methodologies employed in prior studies (Hrysiewicz et al., 2024). Correlation coefficient analyses were performed between time series of displacements measured by SBAS and *in situ* observations for periods corresponding to the *in situ* measurements and divided into three subsets: 1) wet and dry seasons together, 2) dry season and 3) wet season separately. SBAS-derived displacements were linearly interpolated between the S1 acquisitions from 6/12 days to a daily frequency corresponding to the *in situ* frequency, due to the small number of SBAS samples within an analysed season. Next, the linear velocity (vertical displacement rate in cm/year) with RMSE, calculated by least-squares inversion regarding each season (dry, wet, wet+dry), hydrological year and stack length, was analysed.

3.2. SBAS image processing workflow

Monitoring the dynamics of surface deformations using the SBAS approach is possible by obtaining average displacement models and displacement time series from a stack of at least 15–20 SAR images (Crosetto et al., 2016). We adopted two strategies based on the length of time-series, a full stack covering period of six hydrological years (2017–2022) and short stack representing a hydrological year, where each year was independently processed. A previous study adopting an annual subset strategy yielded an improved density of SBAS retrievals

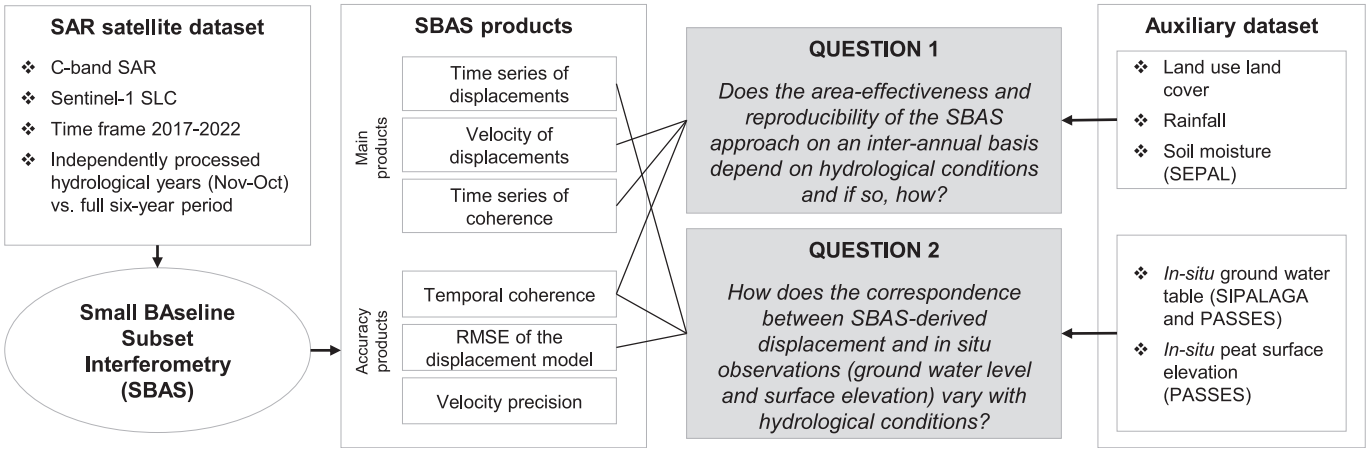

Fig. 4. Conceptual model outlining the project approach.

compared to all-year subsets, explained because this accounted for dynamic surface scattering variations (Izumi et al., 2022b). The hydrological year division *via* the short stack approach allowed us to analyse hydrological conditions in the wet and dry seasons and relate them to SBAS products. The number of acquisitions for the hydrological years ranged from 24 to 29 (Table S1 in supplementary materials) and met the requirements for a minimum number of acquisitions to deal with atmospheric errors. We tested three types of displacements models: linear, quadratic and cubic (noting the technical consideration that quadratic and cubic models, unlike linear ones, require high redundancy and highly coherent interferograms to provide reliable results (Sarmap, 2022), whereas generally areas covered with vegetation are characterised by low coherence (Brisco et al., 2017)). The results of the linear model are presented in the main text, while the results of the other models are presented in the supplementary materials.

The SBAS calculations were performed using the ENVI SARscape® v6.1 software. The full documentation of SBAS procedure can be found in SBAS tutorial by Sarmap – a software provider (Sarmap, 2022). The following processing sequence and parameters were adopted:

1) **Connection graph.**

All Sentinel-1 SLC images from the analysed image stacks were paired (Master and Co-master image), assuming the maximum temporal baseline is 36 days which provides a forward and backward connection to the three nearest acquisitions (12 days is an interval between two consecutive images' acquisitions from a single S1 satellite), and the geometrical baseline does not exceed 5 % of the critical baseline value. When the continuity of the registrations was interrupted, we used three acquisitions forward and backward without limitation to the 36-day assumption to avoid disconnected blocks of interferograms (Fig. S2 in Supplementary Material). Such constraints made it possible to reduce the number of image pairs with poor coherence and shorten the time-consuming calculations whilst providing sufficient interferograms (to build a small baseline subset network, following previous work (Berardino et al., 2002; Cigna and Sowter, 2017; Yunjun et al., 2019; Zheng et al., 2023b)).

2) **Interferometric workflow.**

Once the co-registration was performed, the flattened and filtered interferograms, coherence images, and unwrapped phases were generated using Copernicus DEM GLO-30 and multilooked (1 in azimuth and 3 in range to exploit almost the S1 product's full spatial resolution). The interferograms were filtered using the Goldstein method (Goldstein and Werner, 1998), and coherence was calculated in window size 9 × 9 (to minimise bias during coherence calculation). Delaunay MCF (Minimum Cost Flow - triangular grid) unwrapping method, was used. Delaunay MCF offers greater robustness around areas of low coherence (Sarmap, 2022). A coherence level equal to 0.2 was applied, typical values are stipulated in other studies as being between 0.15 and 0.55 (Berardino et al., 2002; Cigna and Sowter, 2017; Palamà et al., 2022).

3) **Ground Control Point (GCP) selection.**

At the beginning of the next steps (the first and second inversions, and the geocoding), the refinement and re-flattening are automatically performed using GCPs. This step provides GCPs in stable areas. See Supplementary Materials section 2.3 for a detailed description of the GCP selection procedure.

4) **First inversion.**

The refinement and re-flattening were performed using manually selected GCPs (Fig. S3 in supplementary materials). A singular value decomposition (SVD) inversion is performed on the unwrapped interferogram stack to determine a mean displacement rate. Next, the phase of each interferogram is flattened using the estimated mean displacement rate. Subsequently, a second phase unwrapping process is applied to the entire stack.

5) **Second inversion.**

The displacements in Line of Sight (LOS), *i.e.* the date-by-date value [mm] and velocity [mm/year], were generated. The spatial low-pass and temporal high-pass filters (Berardino et al., 2002; Devanthéry et al., 2014; Mora et al., 2003; Sarmap, 2022) were applied to the date-by-date displacements to remove atmospheric phase components. Additionally, related products, *i.e.* RMSE [mm] of the modelled displacements, velocity precision corresponding to the velocity measurement average precision [mm/year], and multitemporal coherence showing how much the displacement trend fits with the selected model, were generated. Outlier values treated as unwrapping errors or atmospheric artefacts are filtered or removed based on inadmissible RMSE in this step.

6) **Geocoding.**

The displacements in slant range geometry (LOS) were converted to vertical displacements by division of them by the cosine of radar wave incident angle and transformed into the geographic coordinate system (EPSG:4326) with a resolution of 15 m by 15 m.

4. Results

4.1. Description of SBAS products

SBAS results for each image stack (linear displacement model) generated a geospatial product showing the ground surface velocity displacements in LOS (Fig. 5). Results for the quadratic and cubic models are shown in supplementary Figs. S4.2-S4.3, respectively. These maps show areas indicating an increase in the sensor-to-target slant range distance in red *vs.* a decrease in the sensor-to-target slant range distance in blue and stability in green. The main area in and around the city of Palangka Raya (2.2°S, 113.9°E) shows temporal stability in surface height in most years. Areas to the North-West (2.2°S, 113.8°E) and South-East (2.3°S, 114.05°E) of the city are more variable in terms of their surface height changes than other regions. Patterns of topographic change are variable from year-to-year with the years 2018–2020 giving very different responses, particularly in the area of improved agricultural land (see also Fig. 1) to the South-West (2.2°S, 113.8°E) of the city, which shows an increase in the sensor-to-target distance in 2018–2019 and a decrease in 2020. As a result of the analysis of the full stack covering the years 2017–2022, the entire study area is stable, with a few places indicating mild subsidence (for example, 2.25°S, 113.95°E). Lack of coherence in the southeastern area of the AOI during 2021 and 2022 year resulted in missing data points (DS – distributed scatterers) for these years (Fig. 6). Conversely, the coherence was consistently close to 1.0 around the city of Palangka Raya through the 2017–2022 time-series meaning that SBAS retrievals were good in this region throughout the monitoring period (Fig. 6).

Crucially to this study, displacement velocity maps (Fig. 5) show different effective retrievals of surface displacement (*i.e.* DS coverage) for each hydrological year. Forest areas and permanent water bodies were excluded from the analyses *a priori* based on annual national land cover maps provided by KLHK. Area distribution and land cover changes within the AOI over analysed years 2017–2022 are shown in Fig. 7c, and land cover maps in Fig. S1 in the supplementary materials. In 2017–2019, the SBAS results covered the biggest areas, from 55 % to 60 % on peat soils and from 33 % to 35 % on other types of soils (Fig. 7a). In 2020 and 2021, the area coverage by SBAS results dropped to around 40 % on peat soils and 25 % on other soils. The lowest area coverage

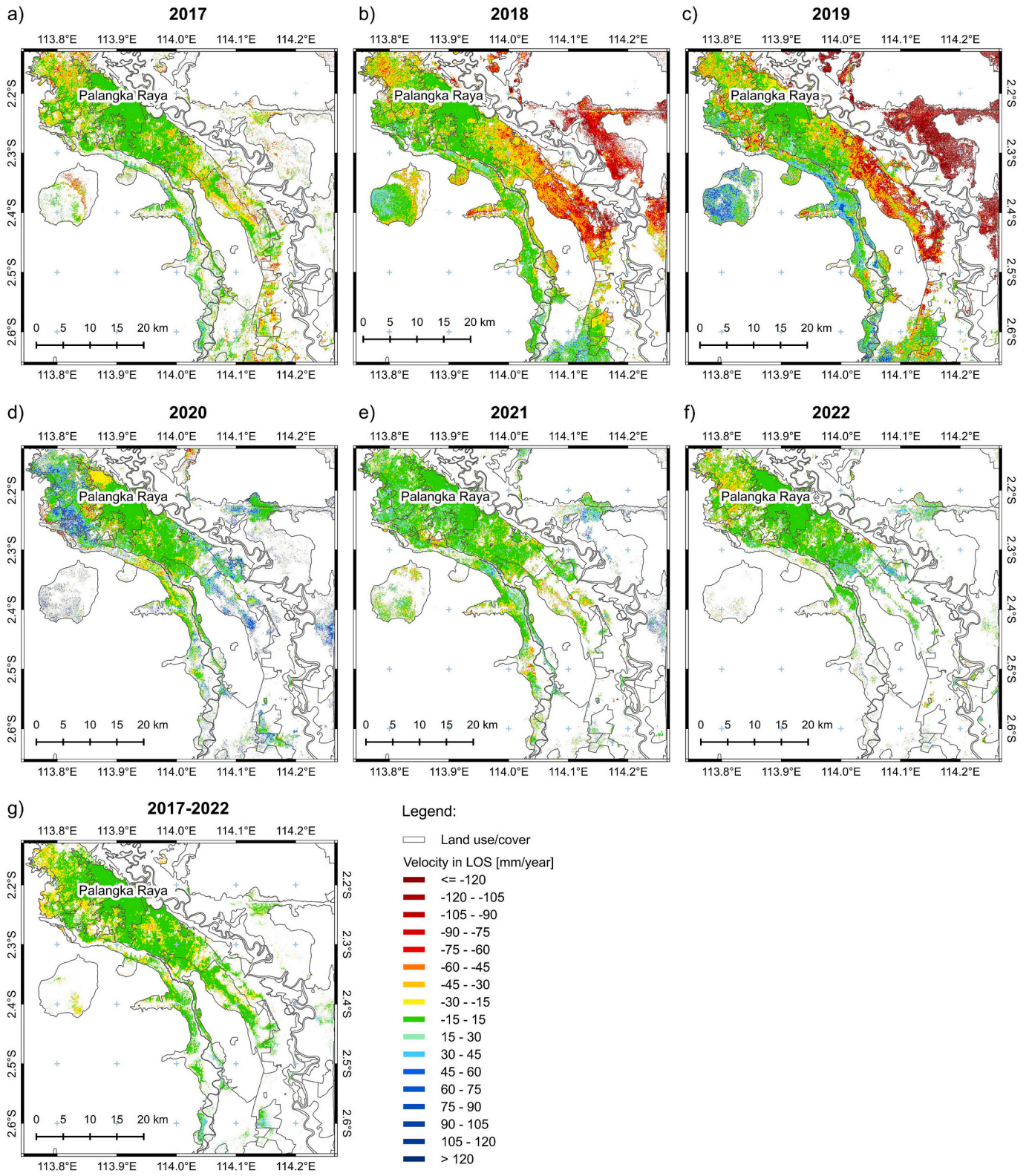

Fig. 5. Map of velocity displacements based on the linear model for a-f) short stacks representing hydrological years 2017–2022, g) full stack. Areas of surface uplift are shown in blue, stable areas in green and subsiding areas in red. (For interpretation of the references to colour in this figure legend, the reader is referred to the web version of this article.)

occurred in 2022 (35 % on peat soils and 20 % on other soils). Note that surface moisture, a satellite-derived metric from the SEPAL project, is shown in Fig. 7d and indicates a change between drier conditions (2017–2019) and wetter conditions (2020−2022).

Considering the area covered by SBAS results in reference to land cover classes, the urban area is covered approximately 99 % throughout the time-series (Fig. 7b). In the years 2017–2019, SBAS results over the peat-covered open ground were 82 %, whilst the soil-covered open

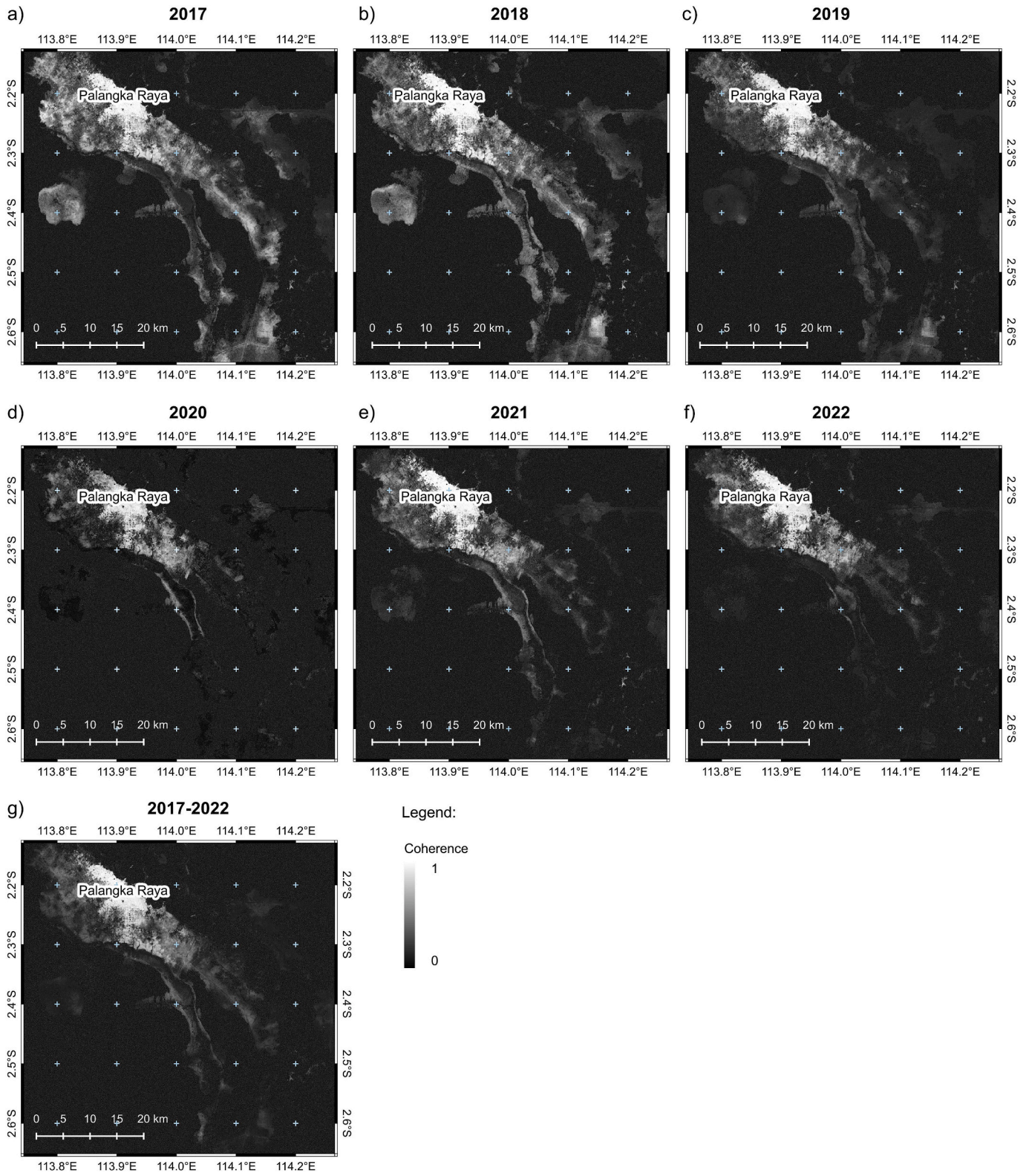

Fig. 6. Map of multitemporal coherence for a-f) short stacks representing separate hydrological years, and g) the full stack covering six hydrological years 2017–2022. This is the absolute, normalised, complex sum of all the flattened (by subtracting the modelled phase) interferograms. The smaller the average residuals in the flattened interferograms, the higher the multi-temporal coherence value until a maximum value of 1 (when the model perfectly fits the measures, and no residuals are left).

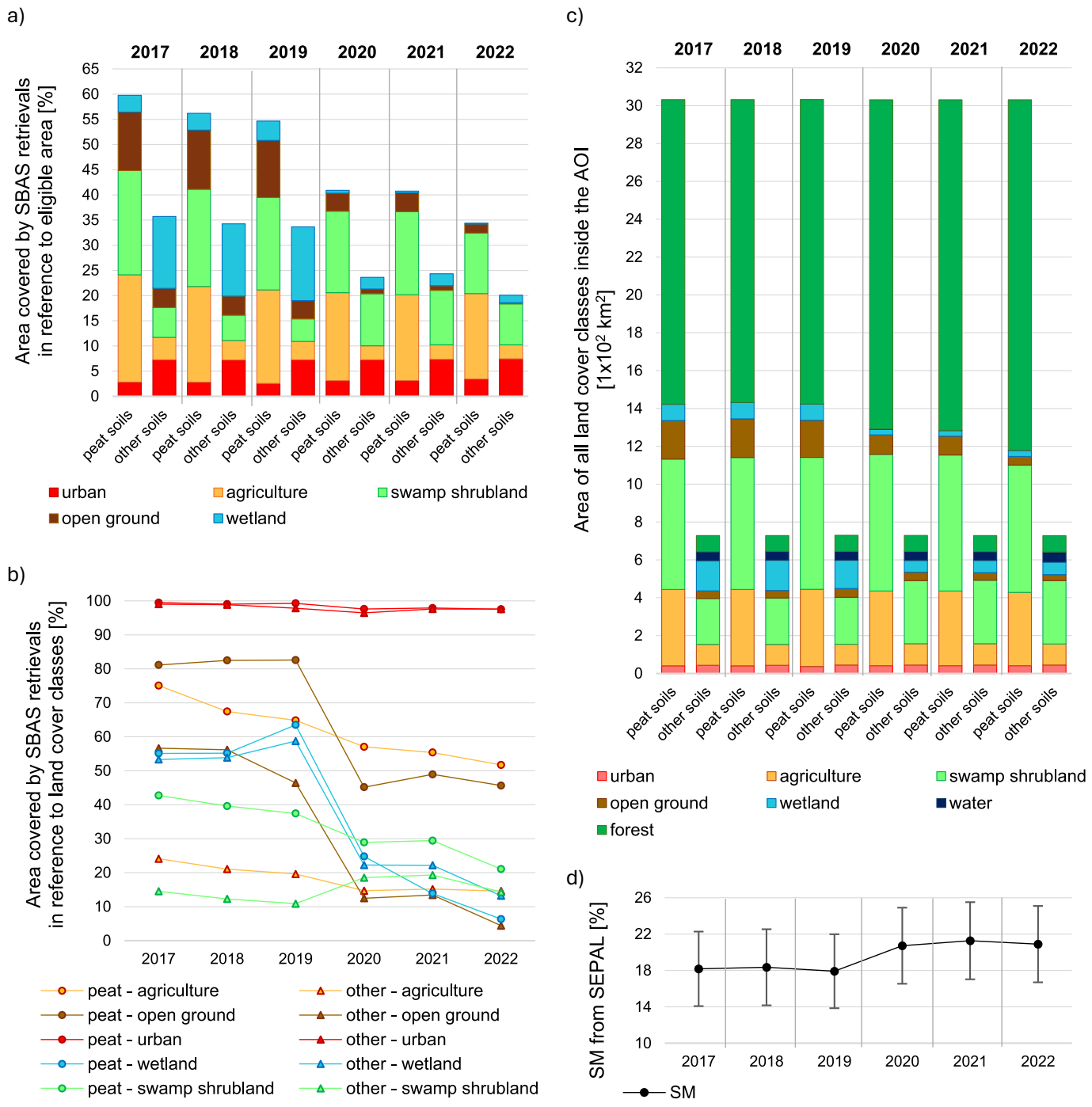

Fig. 7. a) Area of land cover classes (excluding water bodies and forest) inside the AOI covered by SBAS retrievals, b) Area covered by SBAS retrievals in reference to land cover classes and soil type, c) Area distribution of land cover classes within the AOI over separately analysed years from 2017 to 2022, d) soil moisture from SEPAL shows drier conditions 2017–2019 compared to wetter conditions 2020–2022.

ground was lower at 38–43 %. After which, in 2020 and 2021, both decreased (45–49 % for peat-covered and 13 % for other open ground), with further declines in to 4 % for other types of soils in 2022. In turn, coverage of SBAS results in wetlands, independently of soil type was at the same level of 55 % in 2017 and 2018, after which it increased to 60 % in 2019 and fell to 6–24 % in 2020–2022. Coverage by SBAS results over farmlands gradually decreased from 70 % in 2017 to 52 % in 2022 on peat soil and from 24 % to 15 % on other types of soils. A gradual decrease is also noticed for swamp shrubs, from 43 % in 2017 to 21 % in 2022 on peatlands. Coverage by SBAS results over swamp shrubs on other types of soils ranges from 10 % to 19 % over the monitored time period (Fig. 7b).

RMSE maps for the linear model in Fig. 8 (supplementary Figs. S5.2-S5.3 for quadratic and cubic models, respectively) show that the area around Palangka Raya has low RMSE (≤3 mm) throughout the years 2018, 2020, and 2021, indicated by dark blue points. The RMSE for this area increased to 5 mm in 2017, 2019, and 2022. Referencing areas south of the city of Palangka Raya (2.3°S, 114.1°E) affected by subsidence in 2018 and 2019 (Fig. 5b,c), and areas North-West (2.2°S, 113.8°E) showing uplift in 2020 (Fig. 5d) show correspondingly higher RMSE in these years (~10 mm) compared to surrounding areas (Fig. 8b, c,d). Considering the full stack analysis (Fig. 8g), RSME is higher than in

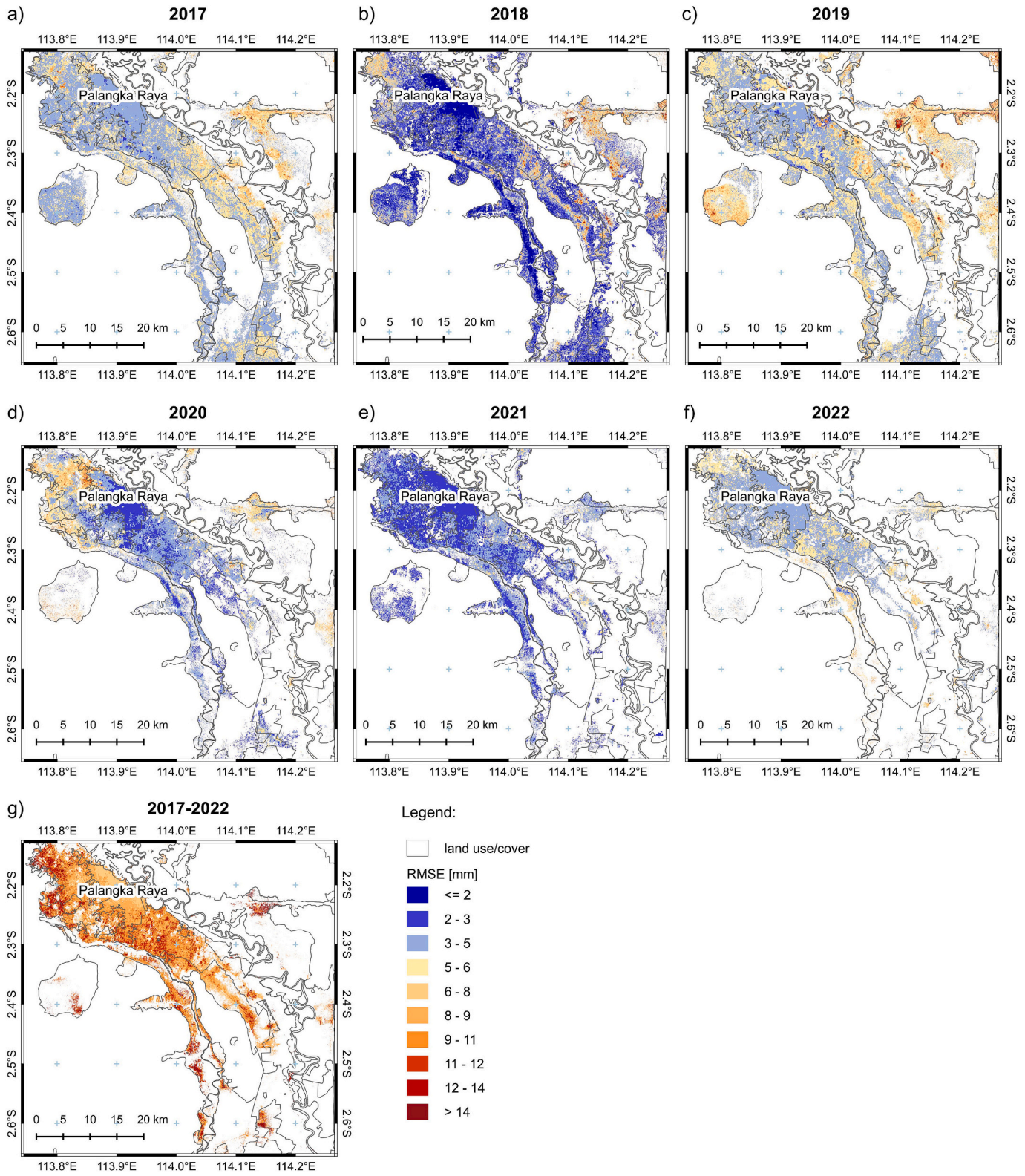

Fig. 8. Map of RMSE showing the fitting quality of the linear displacement model for a-f) short stacks representing separate hydrological years, and the g) full stack covering six hydrological years 2017–2022. RMSE values are presented only for areas where in any hydrological year, the multitemporal coherence was greater than 0.2.

short stacks, showing widespread deviation from the linear model.

4.2. The correspondence between surface hydrological conditions and time series of coherence

The dynamics of SM from SEPAL module and the coherence matrix in

a time series are shown in Fig. 9. Additionally, observed events are marked, *i.e.* the appearance of water above ground level (blue wave icon) and land cover changes due to fire (red flame icon) and forest clearance (four green arrows icon). The coherence matrix indicates coherence for each acquisition in a timeline (0 days on the vertical axis on the right) in reference to the acquisitions behind and ahead 12, 24, and 36 days; in other words, for each SAR pair (SP) used in the SBAS approach. The values of 12, 24, and 36 days result from the S1 satellite imaging interval and are the closest acquisitions. In our work, we adopt the following interpretation to the coherence ranges: 0 – no coherence, 0–0.3 negligible coherence, 0.3–0.5 moderate coherence and 0.5–1.0 high coherence. Discontinuities in the SM plot and in the coherence matrix are related to the lack of data during these periods.

The behaviour of SM dynamics in the time series is similar for all test

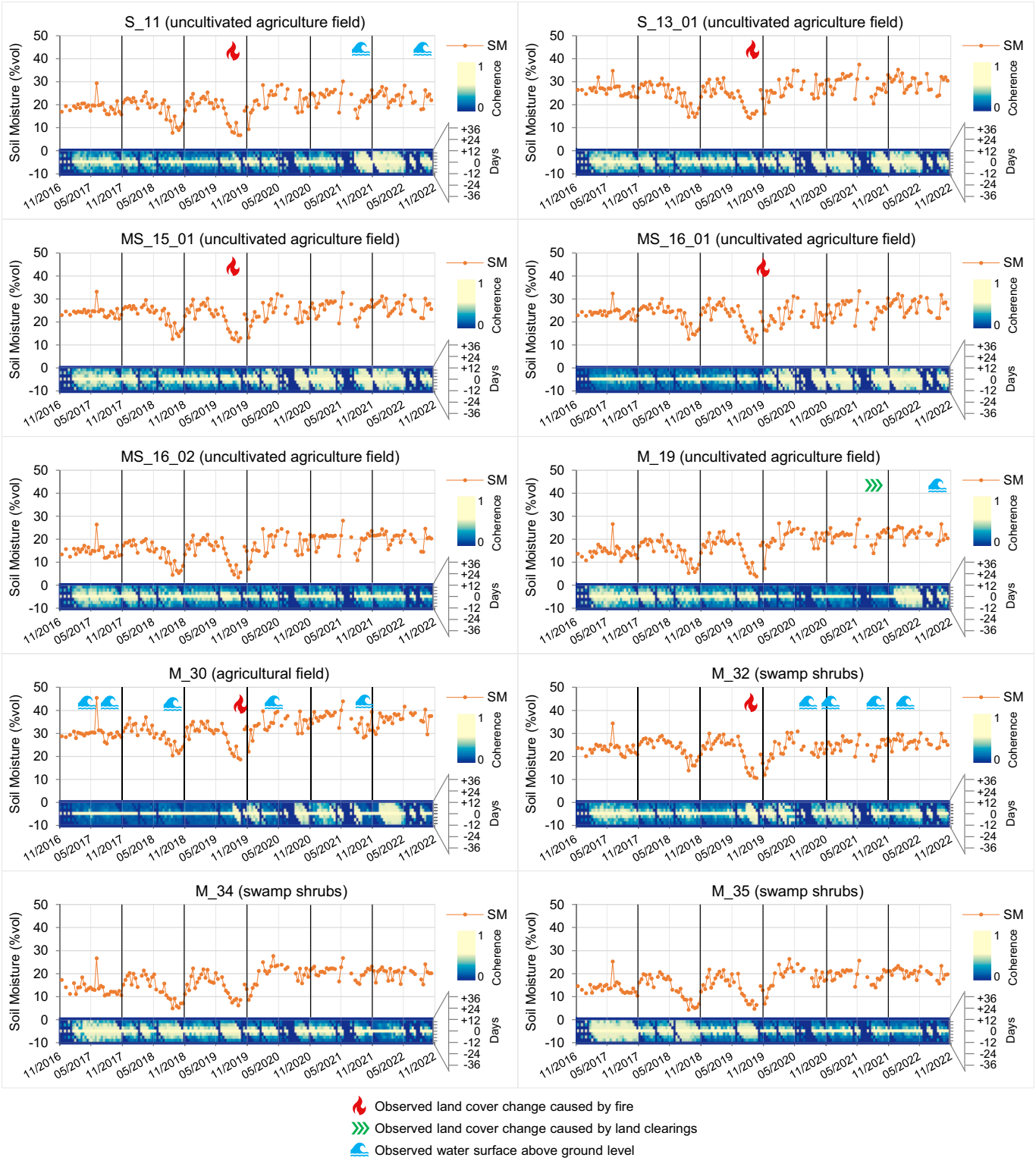

Fig. 9. Time series of soil moisture from the SEPAL module and coherence matrix showing coherence for pairs up to three acquisitions behind and ahead over the whole measurement period.

sites across the six hydrological years from 2017 to 2022. SM was stable during the whole of 2017 with a deviation of 5 percentage points (pp), except June the 3rd, 2017, when heavy rain was recorded. In 2018 and 2019, when rainfall discrepancies between dry and wet seasons were significant (*i.e.* very low precipitation during the dry season and very high precipitation during the wet season, Fig. 3), the negative trend in soil moisture throughout the hydrological year is noticeable. Years 2020–2022 experienced abundant rainfall in both the dry and wet seasons, and these years show the highest SM with a deviation up to 10 pp. The values range from about 5 % in the dry season of 2018 and 2019, up to 45 % for the years 2020–2022.

Moderate or high coherence is seen across the whole analysed period for two test sites, S_13 and MS_15 (uncultivated agriculture). The rest of the test sites are characterised by variable coherence behaviour depending on the season and the hydrological year. There is moderate and high coherence for all test sites and SP with a time-lapse of up to 36 days in 2017, except for test site M_30, with a high water level above the ground, and the wooded agricultural test site M_16_01. In 2018 and 2019, i) the lack of coherence persists for plots M_30 and M_16_01, ii) high coherence is maintained for plots S_11, MS_15, MS_16_02 and M_19, but only for pairs with a time-lapse of 12 days, iii) medium and high coherence for polygons M_32, M_34 and M_35 in the wet season in pairs with a time-lapse of 12 days, and in the dry season with a time-lapse up to 36 days. In the years 2020–2022, i) three test sites show a decrease in the number of SN with moderate and high coherence limited to a maximum time-lapse of 12 days (M_16_02, M_34, M_35), ii) three test sites have moderate and high coherence in pairs with a time-lapse up to 36 days iii) test sites M_30 and M_32 are characterised by variability of high and moderate coherence between wet and dry seasons. In the analysed time series, the relationship of the significant increase in coherence after the fire for the M_16_01, M_30 and M_32 test sites and after clearings in the M_19 test site is clearly visible. A slight change in the increase in coherence is noticeable for S_11, S_13 and MS_15. In general, the occurrence of water above the ground surface coincides with temporally stable high coherence, except for the M_30 test site. A strong dependence of changes in soil moisture on coherence was observed in 2018 and 2019 for test sites M_34 and M_35, not interrupted by fires.

4.3. The correspondence between in situ observations of peat surface and GWL and time series of displacements in tropical peatlands

Due to partial/temporal availability of *in situ* or other hydrological data, the analysis of the comparison of SBAS-derived displacements to *in situ* peat surface and GWL measurements was performed only for the selected hydrological years according to the availability of the data (see Table 2). Only two of the eight available SIPALAGA data measuring stations (BRG_621103_05 and BRG_627104_06) and six peat cameras were located in the vicinity of DS generated from the SBAS approach. Only four test sites had SBAS results that were deemed to be sufficiently reliable when considering the number of points within the 50 m buffer zone (BRG_627104_06, CKAL_001, CKAL_002, CKAL_004, CKAL_005). Measurement points BRG_621103_05, CKAL_003 and CKAL_006 were also included in comparison, but they do lie further from measurement stations (up to 250 m).

The plots (Fig. 10) show time series of vertical ground displacements estimated from SBAS processing (red dots – short stacks, grey dots – full stack), changes in elevation of peat surface (black line), and GWL (blue line) from *in situ* observations. SBAS estimations cover six analysed hydrological years and are calculated as the mean value of displacements of all DS in the given vicinity. Long discontinuities seen in Fig. 10g in the SBAS dots are due to the lack of DS points meeting the criteria of closest vicinity to the measurement station and minimum coherence. Short discontinuities seen around July 2020 and June 2021 are due to the lack of S1 acquisitions in this period. GWL from SIPALAGA observations (BRG stations) span the hydrological year 2019, the wet season 2020, and the dry season 2022. GWL from peat cameras (all CKAL stations) span the hydrological year 2020 and additionally CKAL_002 spans 2021. The peat surface elevation measurements performed by peat cameras cover 2019 and 2020 year.

When combining the correspondence analyses from the various sites in reference to hydrological years (Fig. 11), the correlations between peat surface elevation measured *in situ* and by SBAS (Fig. 11a – short stack, Fig. 11b – full stack) show some linearity particularly for sites CKAL_001, CKAL_002, CKAL_004 and CKAL_005. The correspondence between SBAS-derived surface displacements and GWL is much less clear across a larger number of validation sites (Fig. 11c,d). There is a very clear but site-specific correlation between water table and peat surface elevation (Fig. 11e).

4.3.1. Correspondence between SBAS and in situ measured peat surface displacement

The peat elevation data (Fig. 10a-f, black line) indicate high coherence among sites with no data gaps (CKAL_001, CKAL_002, CKAL_004, CKAL_005, CKAL_006). During the wet season at the start of the hydrological year 2019, all sites exhibited stability (CKAL_003, CKAL_004, CKAL_006) or slight subsidence (CKAL_001, CKAL_002, CKAL_005), followed by sustained subsidence (from 3.06 cm at CKAL_005 up to 6.93 cm at CKAL_001) during the severe dry season until the end of November 2019. Subsequently, all CKAL sites, excluding CKAL_003, rebounded rapidly. CKAL_005 experienced a complete rebound to early 2019 peat elevations, while others had a partial rebound. The less severe 2020 dry season resulted in most sites maintaining stable peat surfaces.

The correlation analysis (Fig. 12) was based on three subsets within each hydrological year: two corresponding to different hydrological conditions identified with wet and dry seasons separately, and one corresponding to the hydrological year - wet and dry seasons together (keeping in mind that the correlation is non-additive, meaning that the correlation of the sum of samples from the wet and dry seasons is not equal to the sum of correlations from the wet and dry seasons).

The correlation coefficients vary significantly across different sites and seasons. In the short stack analysis of the linear displacement model (Fig. 12a), the correlation ranges from no correlation ($r = 0.15$, at site CKAL_002 in the wet+dry season of 2021) to very high correlation ($r = 0.99$, at CKAL_002 in 2019 wet+dry; CKAL_002 in 2019 dry and CKAL_004 in 2019 dry). The full stack analysis (Fig. 12b) shows a similar range, from low correlation ($R = 0.18$, CKAL_003 in 2020 wet season) to high correlation ($r = 0.94$, CKAL_001 and CKAL_002 in 2019 (both wet+dry)).

Next looking at the sign of correlation coefficient in the short stack analysis indicates that correlations in 2019 are consistently positive across various sites (Fig. 12a), while correlations in 2020 are generally negative, with some exceptions for CKAL_003 and CKAL_006 – these sites were located at the greater distance of 300 m from SBAS-retrieval points (Fig. 12a).

Making a comparison of inter-annual responses across hydrological years for short stacks there is a pattern of higher correlation in 2019 than in 2020 for the wet + dry subsets, higher correlations in 2020 than in 2019 for wet subsets, and similar correlation or slightly lower values for the dry subsets in both years 2019 and 2020 (Fig. 12a). Considering the full stack (Fig. 12b), higher correlation coefficients were found in 2019 than in 2020 for the dry and wet+dry seasons, whilst the opposite is true for wet seasons.

Finally, querying the data in Fig. 12a from an intra-seasonal perspective, the correlations vary across different seasons and stack lengths. In general (regardless of sign), the variance is lower for dry seasons than for wet or wet+dry seasons.

The correspondence between measurements from *in situ* and SBAS was also analysed through a relationship of displacement velocity (Fig. 13a,b; Table 3) regarding hydrological seasons (wet, dry and wet+dry). When considering the agreement of displacement directions, most of the wet+dry season direction signs match (Fig. 13a,b; black dots

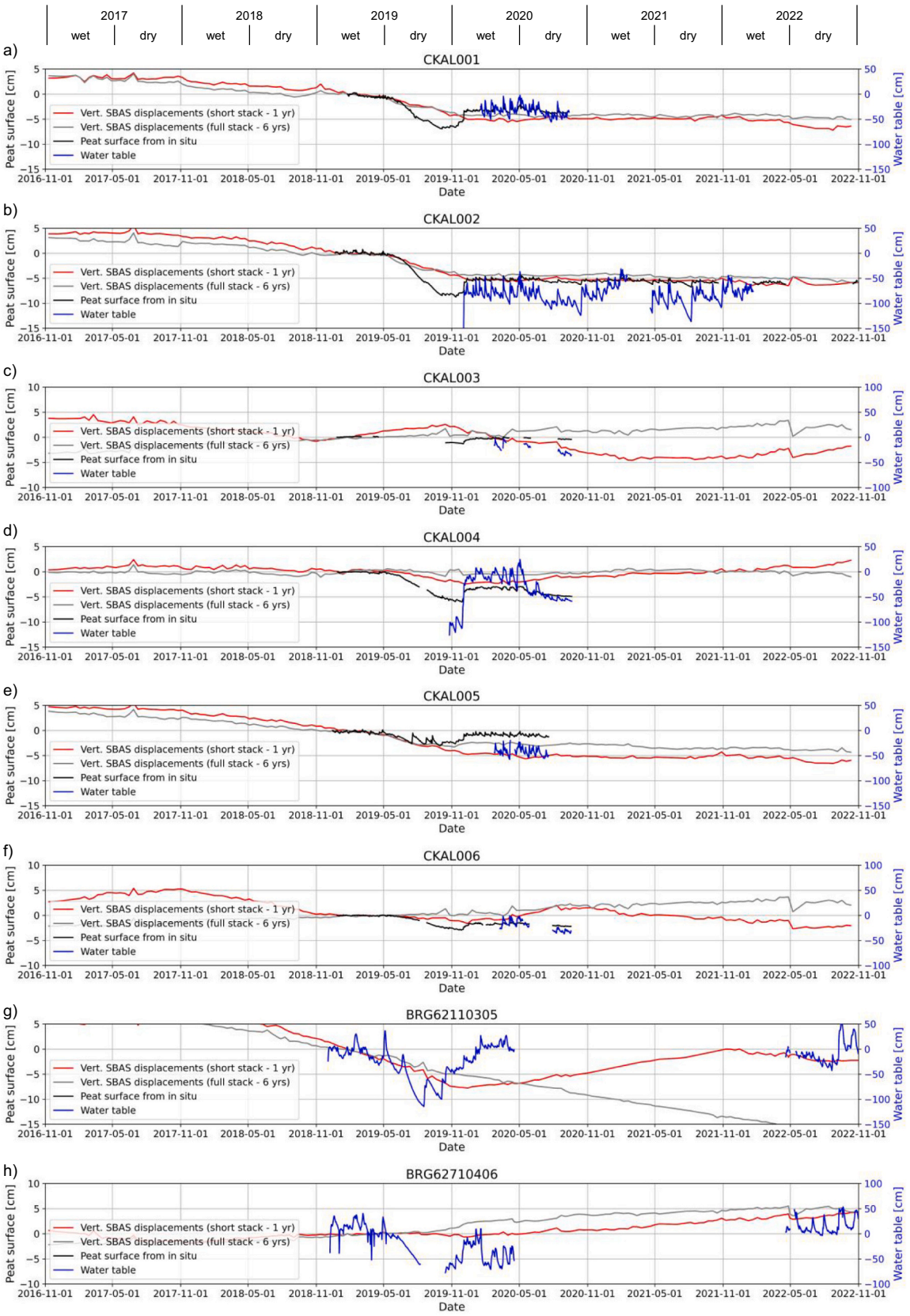

Fig. 10. Time series of peat surface elevation from peat cameras and SBAS-retrieved measurements based on linear model (left y-axis), groundwater level (right y-axis) a-h) for specific test sites. See Fig. S6.1–6.8 in Supplementary Materials for quadratic and cubic models.

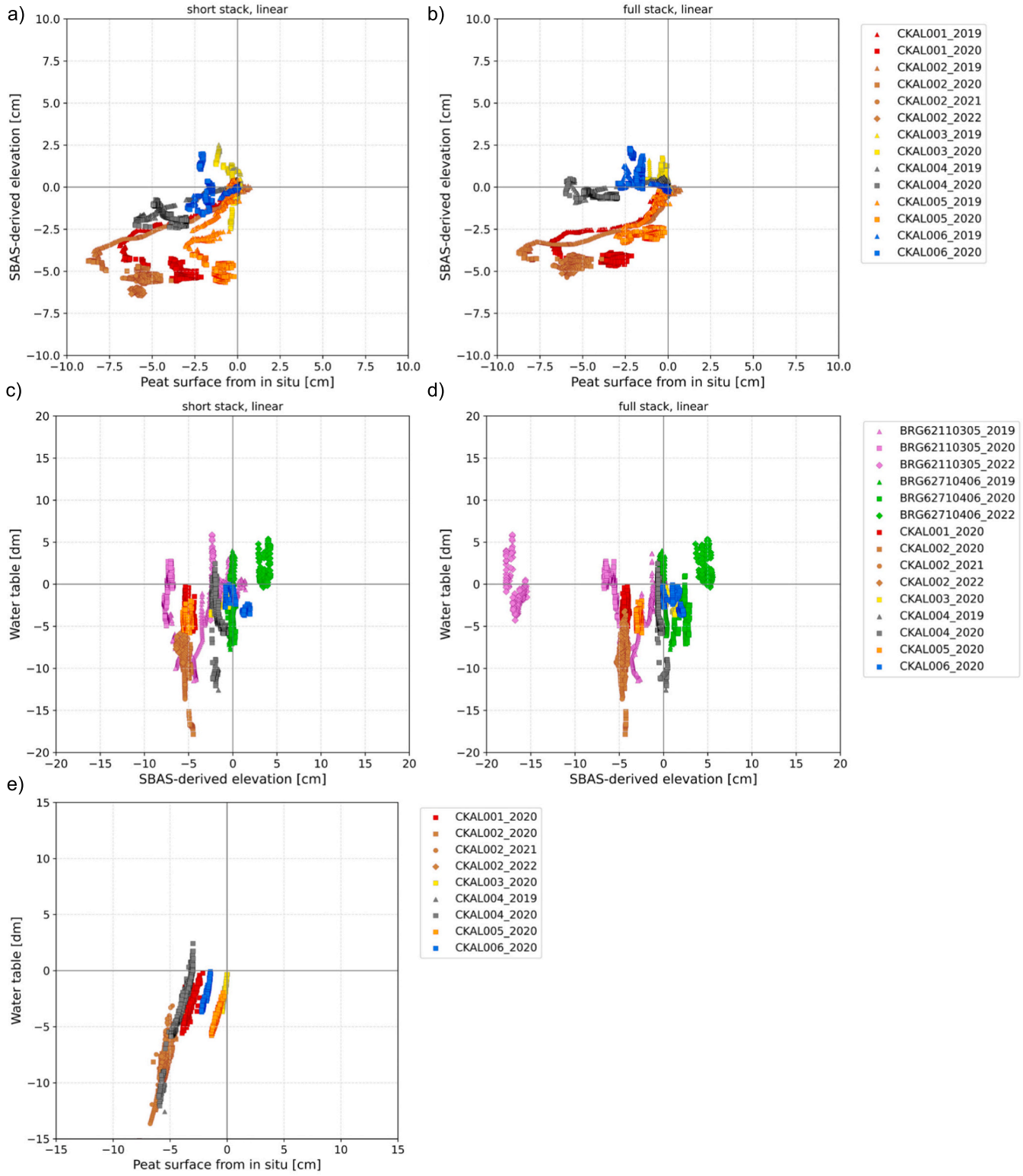

Fig. 11. Scatter plots showing the relationship between, peat surface elevation from *in situ* and vertical SBAS displacements (interpolated between S1 acquisitions dates) for a) short stack and b) full stack; water table and vertical SBAS displacements for c) short stack and d) full stack; e) peat surface elevation from *in situ* and water table for all validation sites.

in the white area of the plots). For the wet and dry season, regardless of stack length, there is a variety (blue triangles and grey squares in the white and grey areas).

Looking at the relationship between the displacement velocity of peat surface changes from *in situ* and SBAS displacements, data are more clustered for full stack (Fig. 13b) than for short stack (Fig. 13a). The error bars (RMSE) show that both the *in situ* measurements and the SBAS displacements have some uncertainty (Fig. 13c,d). Moderate matching of peat surface velocity to SBAS-retrieved velocity is observed for the wet+dry season and full stack (Fig. 13d). Generally, displacement

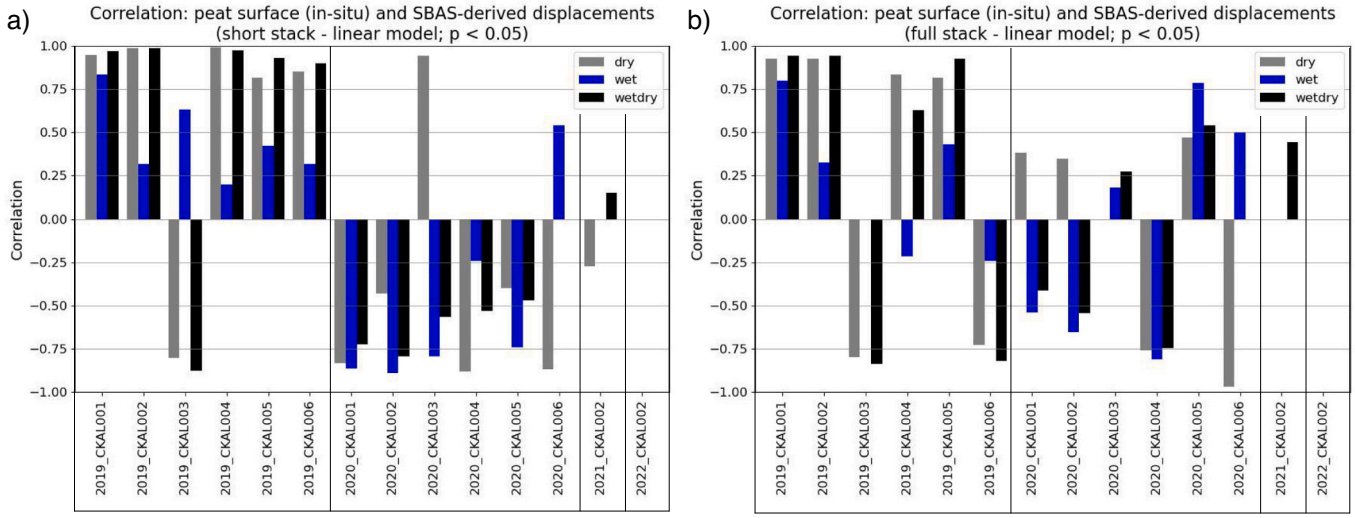

Fig. 12. Correlation between SBAS time-series of displacements and in situ peat surface observations for a) short stack and b) full stack. Statistical metrics are divided into three subsets: wet and dry season together (wet + dry) and dry and wet season separately. Vertical lines separate hydrological years. All presented correlations have *p*-values (statistical significance) less than or equal to 0.05. See Fig. S7 in Supplementary Materials for quadratic and cubic models.

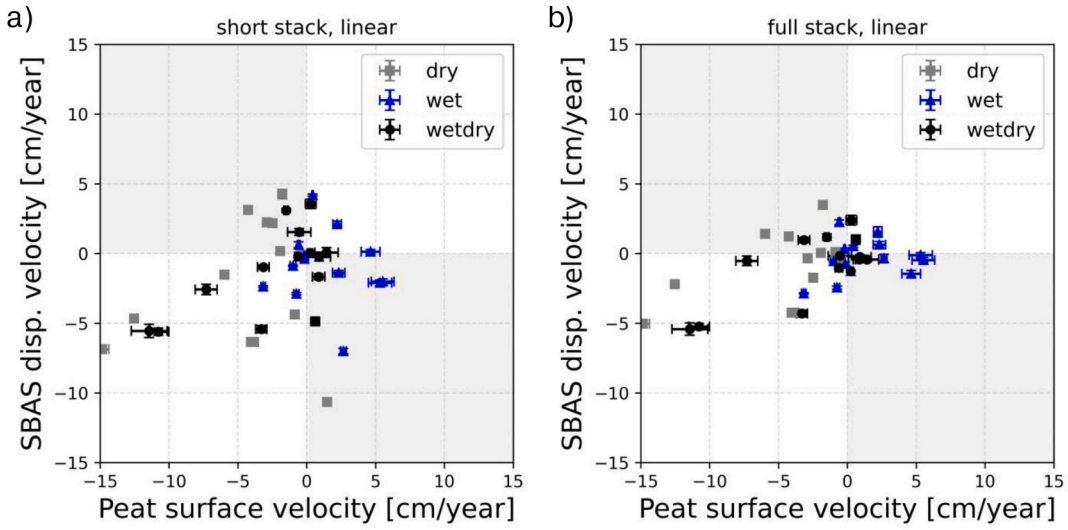

Fig. 13. The relationship between displacement velocity [cm/year] of peat surface changes from *in situ* and SBAS measurements for a) short stack and b) full stack. Error bars represent RMSE. White area means the same directions of velocity, grey area means opposite directions of velocity. See Fig. S9 in Supplementary Materials for quadratic and cubic models.

velocities are higher for SBAS measurements than for *in situ* measurements in dry seasons, and the opposite in wet seasons (Fig. 13c,d).

Analysis of linear seasonal velocities within hydrological years indicates that differences in average peat velocity from *in situ* and SBAS range from 0.21 to 5.49 cm/year for short stack and from 0.08 to 4.02 cm/year for full stack (Table 3), noting RMSE sometimes shows high uncertainty (17.69 cm). The average difference between the peat velocity from *in situ* and SBAS displacement velocity for the dry season is smaller for the full stack (−1.53 cm/year) than for the short stack (−3.05 cm/year). Similarly to the wet season, where the average difference is 2.12 cm/year and 1.61 cm/year for short and full stack, respectively (Table 3). Taking into account the wet+dry season the average difference in velocities is slightly smaller for short stack than for full stack.

Statistically, comparing seasons (Table 4) and looking at Pearson's coefficient in the dry season, there is a moderate positive correlation between peat and SBAS velocity for short stack (0.41), no correlation for full stack (−0.11). During the wet season there is weak correlation with both short and full stack (Table 4). In turn, there is a strong positive correlation in wet+dry between peat and SBAS velocity for full stack (0.73) and moderate for short stack (0.62). Considering the paired-samples *t*-test, $p < 0.05$ indicates a statistically significant difference between the SBAS modelled velocity and *in situ* peat measurements. The difference between peat velocity and SBAS velocity for full stack in wet season is significant ($p = 0.043$). No significant differences ($p > 0.05$) is for other seasons, but wet (short stack) is close to the threshold.

4.3.2. *Correspondence between SBAS and groundwater level*

Throughout the analysed period, groundwater level fluctuates (in Fig. 10) and varies from site-to-site. At sites CKAL_001, CKAL_002 and CKAL_005, GWL rapidly fluctuates with 0.25 m amplitude from February to July 2020, keeping an overall stable trend. At site CKAL_004, the range of fluctuations rises until the beginning of the dry season of 2020, after which it decreases. During the transition from the

Table 3
Summary of the average differences in velocity displacements and RMSE, estimated from the SBAS approach and velocity of peat surface from *in situ* measurements in reference to the analysed hydrological season and stack length.

Season	Hydroyear	Peat velocity from *in situ* and SBAS displacements velocity (short stack, linear model)		Peat velocity from *in situ* and SBAS displacements velocity (full stack, linear model)	
		Average diff. [cm]	RMSE [cm]	Average diff. [cm]	RMSE [cm]
dry	2019	−2.92	8.53	−0.50	17.69
dry	2020	−3.63	5.09	−2.83	3.40
dry	2021	−0.33	0.33	0.08	0.08
dry	whole analysed period	**−3.05**	**6.75**	**−1.53**	**12.24**
wet	2019	−0.62	1.86	−0.42	1.39
wet	2020	5.49	6.32	3.82	4.38
wet	2021	0.23	0.23	0.58	0.58
wet	2022	0.21	0.21	1.50	1.50
wet	whole analysed period	**2.12**	**4.31**	**1.61**	**3.04**
wet+dry	2019	−3.40	4.36	−4.02	4.80
wet+dry	2020	0.87	3.02	0.24	1.37
wet+dry	2021	−0.39	0.39	0.42	0.42
wet+dry	2022	0.21	0.21	1.50	1.50
wet + dry	whole analysed period	**−1.10**	**3.47**	**−1.48**	**3.29**

Table 4
Summary of the t-test comparing averages and Pearson's coefficient assessing the strength and direction of the linear relationship between displacement velocity of peat surface changes from *in situ* and SBAS displacements.

	Peat *vs* SBAS (short stack) velocity of vertical displacement			Peat *vs* SBAS (full stack) velocity of vertical displacement		
Season	t-test	p value	Pearson's coefficient	t-test	*p* value	Pearson's coefficient
dry	−1.75	0.10	0.41	−0.44	0.67	−0.11
wet	2.03	0.06	−0.13	2.25	0.04	0.22
wet+dry	−1.20	0.25	0.62	−1.82	0.09	0.73

dry to the wet season in 2020, the CKAL_004 experienced a significant 1 m GWL drop. At site CKAL_003, no fluctuations are visible due to the discontinuity of the acquired data. At sites BRG_621103_05 and BRG_627104_06 in 2019 and 2020 there is a clearly visible decrease in GWL between the wet and dry seasons (Fig.10g-h). At points BRG_621103_05 and BRG_627104_06 in the wet season of 2019 the GWL fluctuations are significant, and their amplitude varies 0.5 m above and below the ground. At site BRG_621103_05 during the dry season 2022, the groundwater level decreases until mid-September, after which the water rises to above the ground and rapidly fluctuates (twice between mid-September and the end of October). During this time, the water level above the soil surface fluctuated between 0 and 50 cm within two weeks (Fig.10g). In the case of the site BRG_627104_06, the water level above the soil surface varies from 10 cm to 50 cm within two week periods throughout the dry season (Fig. 10h). Looking at the co-located GWL/peat stations (Fig.11e), as the water level below the soil surface decreases, the peat surface level decreases (Fig. 11e, markers below zero on the x- and y-axis). When the water level is above the ground, the peat surface level remains at the same level (Fig. 11e – grey markers above zero on the y-axis).

The correlation coefficients considered to be statistically significant ($p < 0.05$), between GWL from *in situ* and SBAS measurements vary significantly across different sites, years and seasons. A span of correlation values and variability occurs from 0.2 to 0.99 (Fig. 14 and Tables S3a,b).

Looking at the sign of the correlation coefficient, the analysis shows a mixed pattern in the sign of the correlation coefficient for all stack lengths. Correlations in 2019 are consistently positive across various sites for the short linear model (Fig. 14a), while correlations in 2020 are generally negative, with some exceptions for CKAL_003, CKAL_006, and BRG_621103_05 located at the greater distance of 300 m from SBAS-retrieval points.

For most of the test sites for the short stack, linear model (Fig.14a) for which the water level above ground level was observed throughout the analysed period (Fig. 14d), and especially for the dates corresponding to the S1 acquisition dates (Fig. 14c), a lack, low correlation or $p > 0.05$ is noticeable (see supplementary Table S3a,b). The exception is the BRG_621103_05 site in 2019, which had a correlation range of 0.72 (dry, wet+dry) to 0.77 (wet).

Considering the displacement velocity, the velocity of the GWL changes within the season is several times larger than the velocity of the SBAS-derived displacements (Fig. 15a-b). Considering the displacement directions, generally, co-located stations with both GWL and peat *in situ* measurements (Fig.15c) show agreement in displacement directions for wet (positive values) and dry season (negative values), but taking into account dry+wet season, displacement directions don't match (black dots). In overall SBAS and GWL measurements at all validation sites, the displacement directions are more various and velocities are site-specific, not season-specific (Fig. 15a,b).

5. Discussion

5.1. Does the area-effectiveness and reproducibility of the SBAS approach on an inter-annual basis depend on hydrological conditions and if so, how?

The fundamental limitations of SBAS Interferometry using C-Band Sentinel-1 data, resulting from short wavelengths and scattering mechanisms in the natural environment, are related to areas where the land cover is forest and open water. C-band wavelengths interact mainly with upper sections of the forest canopy and are characterised primarily by volume scattering that does not show high enough level of the phase coherence required for InSAR measurements. Surface waters are by definition excluded from interferometric analyses. In our work, restricted to tropical peatlands and wetlands covered by vegetation (Fig. 7c and Fig. S1 in supplementary materials), the area-effectiveness of the SBAS approach was variable within individual classes and its changes should be interpreted as changes in the proportionate retrievals of surface information with respect to those land use classes, *i.e.* from year to year there are fluctuations in successful SBAS retrievals across the site (Fig.7b). This highlights the operational challenges with applying SBAS to the study of surface displacements in areas with complex and heterogeneous land cover. The SBAS approach using C-band SAR has been demonstrated to be able to obtain retrievals of surface displacement from 34.5 % to 60 % of eligible distributed scatterers within the peat soils (from 390 to 826 km^2) and from 20 % to 55 % within other types of soils of the AOI depending on the hydrological year analysed (Fig. 7a). It is not possible to compare fully these values with other works because of specificities in the land cover of different sites, differences in the way that retrievals are reported (*e.g.* some studies report densities of points per km^2 (Zhang et al., 2019)), differences in output pixel size across studies, and in analysed time-frame, which will deliver different outcomes. However, we see the same pattern of displacements and reduction in the number of coherent scatterers, which is consistent with the results obtained in the same area in Central Kalimantan as in Izumi et al. (2022b) work.

Several important factors, such as i) input data inconsistencies, ii) processing parameters inconsistencies, iii) transmitting and receiving SAR signal delay (Doin et al., 2009), and iv) volume scattering and temporal changes of ground objects, might cause differences in the area-effectiveness and reproducibility of the SBAS approach over the same

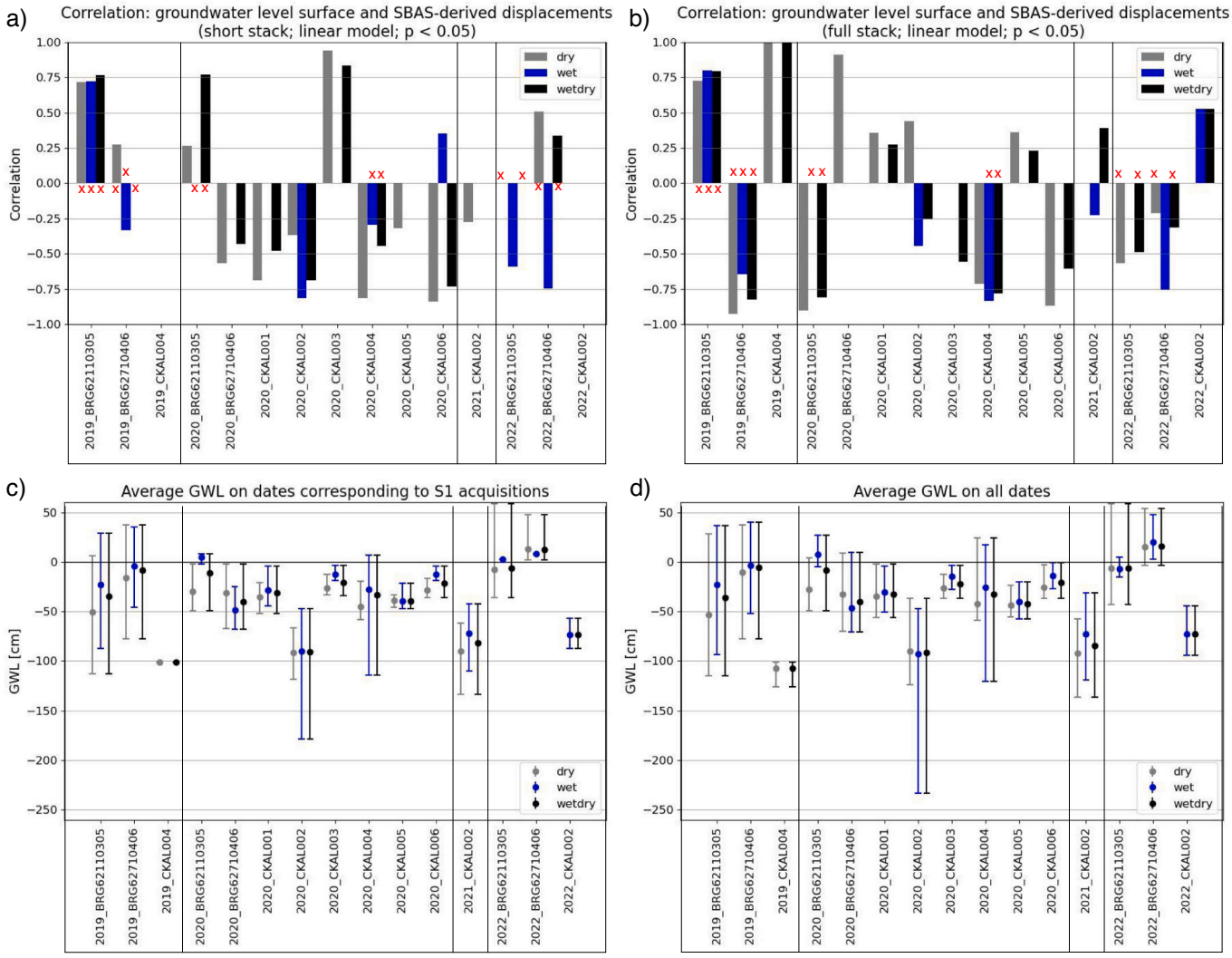

Fig. 14. Correlation between time-series of displacements measured by SBAS and *in situ* observations groundwater level observations for a) short stacks and b) full stack. Test sites with water above ground level are marked with x (red); c) Mean, minimum and maximum groundwater level measured for dates corresponding to S1 acquisitions; d) Mean, minimum and maximum groundwater levels measured for all dates within the analysed period. Statistic metrics are divided into three subsets: wet and dry season together (wet+dry) and dry and wet season separately. Vertical lines separate hydrological years. *All presented correlations have p*-values (statistical significance) less than or equal to 0.05. (For interpretation of the references to colour in this figure legend, the reader is referred to the web version of this article.)

area. This assumes that the other decorrelation sources are reduced by using the SBAS technique (Berardino et al., 2002), as mentioned in Section 3.1. In our approach, we used a similar input dataset (number of images, image distribution in spatiotemporal baseline network, number of interferograms, number of connections), the same processing parameters (coherence threshold, unwrapping method *etc.*), plus we removed atmospheric delay by spatiotemporal filtering at the second inversion. Therefore, we identify the volume scattering and temporal changes as the main reason for differences in the area-effectiveness and reproducibility of the SBAS approach on an inter-annual basis. Within this we can distinguish land cover changes (*e.g.* vegetation growth, fires, land management), hydrological peatland condition (*e.g.* soil moisture, water table level, inundations), and climate/weather (*e.g.* rainfall, wind). Some studies also underline that microtopography (hummocks and hollows) could be associated with distinct peat surface motion behaviours in temperate peatlands (Marshall et al., 2022). In our work, we include annual land cover maps for each calendar year from 2017 to 2022, and we perform analyses within a given class, presenting results as percentages rather than absolute values. Therefore, we do not identify changes in the general land cover classes as sources of SBAS retrieval reduction. Although the distribution and area size of the land cover class changes (Fig. 7c), which can also be seen on the maps in Fig. S1, we don't connect this with a change in the area covered by SBAS retrieval. Some classes indeed show a relationship between the reduction of the class area and the reduction of the number of SBAS retrievals. For example, the open ground area on peat soils and the wetland class decreased in 2020 (Fig. 7c), as did the number of SBAS retrievals (Fig. 7b). In contrast, the open ground area on other soils remained the same, and the number of SBAS retrievals decreased. The area of agricultural land, neither on peat nor other soil, did not change (Fig. 7c), and the number of SBAS retrievals decreased (Fig. 7b). Izumi et al. (2022b) indicate that massive seasonal fire events and vegetation growth mainly cause decorrelations, we demonstrate that hydrological conditions play an important role in it as well (Fig. 9). As described in Section 4.1, displacement velocity maps (Fig. 5) show different effective retrievals of surface displacement for each hydrological year. We presented that the area coverage depends on the multitemporal coherence shown in Fig. 6. In the southeastern part of Palangka Raya (2.6° N, 114.1° E), there was a loss of temporal coherence in 2020–2022 compared to 2017–2019 consistent with higher soil moisture variations respectively (see SEPAL

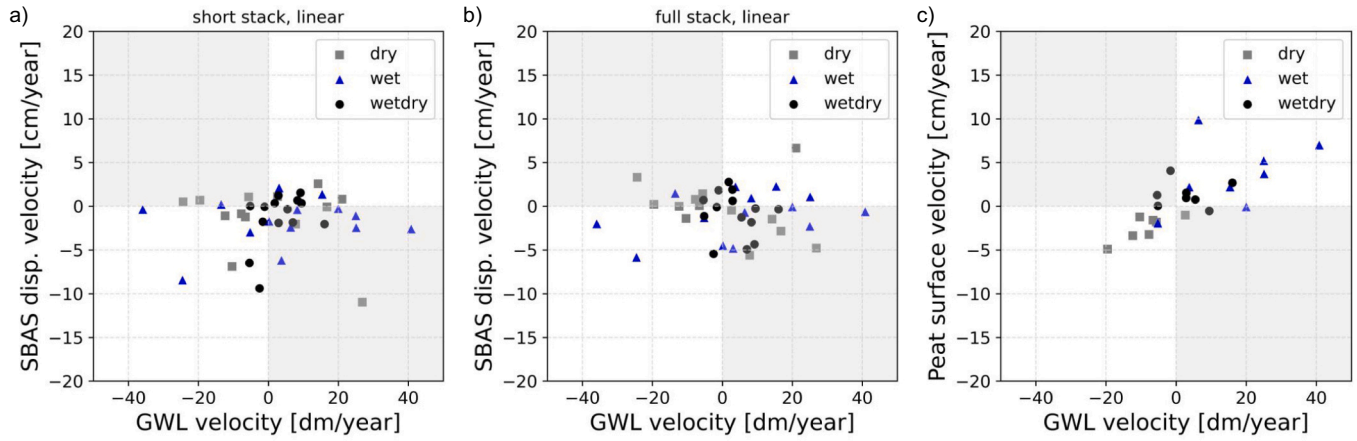

Fig. 15. The relationship between displacement velocity of groundwater level changes from *in situ* and SBAS displacements for a) short and b) full stack,; c) relationship between displacement velocity of groundwater level changes and peat surface elevation only from collocated *in situ* sites. White area means the same directions of velocity, grey area means opposite directions of velocity. See Fig. S10 in Supplementary Materials for quadratic and cubic models.

data (Fig. 9) and please bear in mind that there were no land cover class changes (Fig. S1 in supplementary materials)). This would mean that during periods of conditions when swamps display extreme variability due to the strength of episodic water inputs *i.e.* rain (Price et al., 2023), effective retrievals of surface displacement are weaker. The relationship between loss of coherence and soil moisture variations has already been demonstrated in many works (Hrysiewicz et al., 2023; Scott et al., 2017; Zwieback et al., 2015). Additionally, we noticed that loss of the multi-temporal coherence in our case study was consistent with an increase of the soil moisture absolute values (Fig. 7d).

In this study we analysed in detail the evolution of coherence in time and sources of temporal decorrelation for ten representative test sites, as phase coherence is the essential requirement for InSAR analysis. Several general patterns can be identified based on test sites (Fig. 9):

- In wetter conditions, coherence is impacted and this is fairly consistent regardless of land cover. At the test sites that did not suffer from fires in 2019 (M_16_02, M_34, M_35, and M_19 until land clearings in 2022), there is an apparent decrease in coherence from 2020 as the time interval between S1 acquisitions increases (Fig. 9). After 2020, an increase in the average groundwater level was noted. GWL oscillated between 0.5 m above and − 0.5 m below ground (Fig. 10), unlike in 2019, from 0.5 m even to −1.5 m below ground.
- Wetter conditions also influence inter-seasonal coherence (between wet and dry seasons). When surface water significantly fluctuates above the ground in the wet season, the coherence is not sustained for a long time (only for the closest S1 acquisitions, Fig. 9), whilst the opposite is the case during the dry season (M_34, M_35 in 2018–2019) when coherence is preserved for longer intervals between acquisitions. Tampuu et al. (2020a) also reported a relationship between seasonality and decorrelation in temperate peatlands. Open bogs showed a better correlation when the GWL difference between the acquisitions was reduced (Tampuu et al., 2020a).
- In swamp sites (*e.g.* M_34, M_35; Fig. 9) with no floods (water above the vegetation) or fires during the time sequence, dry periods correspond directly to improvements in coherence. This is not reflected as strongly in agricultural sites M_16_02 and M_19 (Fig. 9), although those sites were likely to be more dynamic in terms of land cover changes.
- Fire, which occurred in the very dry season of 2019 generally increased coherence because vegetation was removed, delivering greater likelihood of double bounce from lying tree trunks (M_15, M_16_01; Fig. 9).

5.2. How does the correspondence between SBAS-derived displacement and in situ observations (ground water level and surface elevation) vary with hydrological conditions?

Previous studies have demonstrated time-series comparison of InSAR-derived displacement over non-tropical peatlands using *in situ* peat surface elevation (Marshall et al., 2022; Tampuu et al., 2023) or peat surface with groundwater level (Hrysiewicz et al., 2024; Hrysiewicz et al., 2023). Umarhadi et al. (2021) extended this approach to tropical peatlands by converting GWL data to surface elevation. However, our study is the first to directly validate InSAR results in tropical peatlands using collocated measurements of both GWL and peat surface elevation. Unlike prior work, which did not report substantial above-ground water fluctuations, our study accounts for seasonal hydrological variability, including periods when water levels exceed the ground surface. Given that SAR signals reflect the first surface encountered, this variability introduces uncertainty in interpreting displacement signals. We therefore compare GWL and peat surface data to assess the influence of hydrological conditions on SBAS-derived displacements across seasons and hydrological years.

5.2.1. Relationship between SBAS displacements and peat surface measurements

Reported average difference between InSAR and *in-situ* peat velocity over non-tropical peatlands was 1.6 cm/year for Marshall et al. (2022), 2.9 cm/year for Tampuu et al. (2023), 0.7 cm/year for Hrysiewicz et al. (2024), and tropical peatlands from 1.5 to 2.1 cm/year (depending on land use class) for Umarhadi et al. (2021). Our study showed a mismatch from 0.21 to 5.49 cm/year for short stack and from 0.08 to 4.02 cm/year for full stack for different seasons (Table 3). At this point, supporting the findings of Hrysiewicz et al. (2024), we confirm that shorter time-series are associated with greater discrepancies. Analysis of hydrological seasons shows that the wet+dry season is slightly better estimated using short stack (−1.10 cm/year) than full stack (−1.48 cm/year), as shown in Tables 3 and 4. In the dry season, although the difference in velocity for the short stack is twice as large (−3.05 cm/year) as for the full stack (−1.53 cm/year), the uncertainty is significantly larger for the full stack (12.24 cm/year). In the wet season, difference in velocity for the short stack (2.12 cm/year) is slightly lower than for full stack (1.61 cm/year), but based on *t*-test the difference between peat velocity and SBAS velocity for full stack in wet season is significant (0.43), while for short stack is close to the threshold (0.06). The full stack analysis also shows a more mixed pattern in the sign of the correlation coefficient of displacements, compared to short stacks (Fig. 12). Moreover, in accordance

with the work of Izumi et al. (2022b), we have shown that the use of long time series leads to a significant loss of the number of SBAS points (Fig. 5) as well as to the loss of fluctuation dynamics in some model cases (supplementary Figs. 4.1–4.3), explaining these patterns. Displacement estimates derived from SBAS show seasonal biases, with consistent underestimation during dry periods and overestimation during wet seasons across all models and stack types. This pattern aligns with previous studies (Alshammari et al., 2018; Marshall et al., 2022; Tampuu et al., 2023), which also reported displacement underestimation under drought conditions. The most pronounced underestimation in our study occurred in 2019 (Fig. 10a,b,d), regardless of the stack length or displacement model used.

In addition to the quantitative accuracy analysis, we examined the trends of the displacements from *in situ* and SBAS measurements. At some sites, trends did not agree. For example, CKAL_001, CKAL_002, CKAL_004, CKAL_005 showed high negative correlations between peat surface and SBAS displacements in all season subsets in 2020 (Fig. 12a). For CKAL_001 and CKAL_005, this mismatch likely results from high-frequency hydrological fluctuations near the surface (Fig. 10a,e) combined with phase unwrapping uncertainties - potentially interrelated factors requiring further investigation. In CKAL_004 the explanation is more likely to be driven dominantly by hydrological effects; the correlation switches here because of surface water being present above the ground, causing the SBAS method to measure changes in water level rather than changes in the elevation of the peat surface (*e.g.* in Fig. 12a the peat level remains stable while the water level fluctuates above the ground). Additionally, soil moisture variations can affect radar phase, introducing displacement errors of 10–20 % of the radar wavelength (Zwieback et al., 2017).

5.2.2. Relationship between SBAS displacements and GWL measurements

Groundwater level (GWL) is recognised as the primary driver of peat surface displacement (Evans et al., 2021; Ledger et al., 2023), and our test sites confirm this with a clear linear relationship between GWL and peat surface elevation (Fig. 11e). However, the correlation between SBAS-derived surface displacements and GWL is less clear across validation sites and varies by location (Fig. 11c,d). For example, at BRG_627104_06, BRG_621103_05, CKAL_001, and CKAL_004, GWL fluctuates without a corresponding SBAS response. This discrepancy likely stems from site-specific hydrological complexity and land cover differences (Fig. 2), as well as the smoothing effect of SBAS filtering, which may oversimplify highly variable water table dynamics (Fig. 10). Therefore, model selection is critical. No single approach suits all conditions, and models must be tailored and validated for each study period (see supplementary Fig. S6-S7). Currently, many improvements to the fundamental SBAS approach have been developed (Li et al., 2022b), including the integration of machine learning for InSAR time series, *e.g.* through the automated selection of high-quality interferograms, which improves displacement accuracy and reduces noise (He et al., 2021).

The SBAS approach, designed for detecting subtle surface changes, may not detect large water level changes above ground (*e.g.*, flooding), especially when rapid fluctuations occur between Sentinel-1 acquisitions. For instance, at site BRG_627104_06, a 40 cm change in water level within two weeks has been recorded (Fig. 10c), highlighting the influence of hydrology on displacement responses. We also didn't observe rapid deformation due to peat loss, although significant subsidence (51 cm) linked to fire was reported in 2019 (Kusin et al., 2020). Furthermore, the southeastern area of Palangka Raya, represented by test sites M_34 and M_35, shows that multitemporal coherence in the years 2020–2022 is low, while phase coherence occurs but is limited to the maximum time-lapse of 12 days between SAR acquisitions. This may mean soil moisture variations or periodic fluctuations in the water level in the analysed period, with the high RMSE constituting evidence for this (supplementary Figs. S5.1–5.3). The solution to this can be found in the synergy of multi-frequency and multi-mission SAR data (*e.g.*, Sentinel-1, NISAR, ROSE-L, Biomass) that will provide richer temporal and spatial coverage, enabling more robust monitoring of dynamic peatland processes.

To overcome the limitations of InSAR in tropical peatlands due to vegetation presence, several advanced methods are emerging. Missions like Biomass (launched in 2025), operating in P-band, are expected to significantly enhance subsurface sensitivity, though they will require complex processing techniques such as Tomographic SAR (TomoSAR). TomoSAR offers the potential to resolve vertical scattering structures, which is particularly valuable in forested peatlands where volume scattering dominates. Polarimetric InSAR (PolInSAR) can further improve discrimination between canopy/vegetation and ground signals, aiding in more accurate displacement retrieval.

6. Conclusions

SBAS interferometry using Sentinel-1C-band data has previously been shown to be useful for determining peatland surface displacements and thus potentially can be a tool for providing proxy values for eco-hydrological parameters critical in peatland restoration. Nevertheless, natural areas covered with vegetation are still a challenge in the use of InSAR, especially when working on short wavelengths (*e.g.* C-band) and new methods or improvements are being sought to provide higher accuracy and area efficiency. Regardless of the method chosen, ground target-based decorrelation sources exist. Our study aimed to fill the gap in studies about the role of hydrological tropical peatland conditions, which can change more dynamically than temperate peatlands, *i.e.*, the amplitude of fluctuations is higher. This is potentially a source of temporal decorrelation in SBAS-derived measurements with potential to introduce errors in the estimated deformations. Results from this work are the first to show that when surface water significantly fluctuates above the ground in the wet season, the coherence is not sustained for a long time. This is the opposite of the dry season, when coherence is preserved for longer intervals between acquisitions. The range of correlation values between SBAS-derived displacements and *in-situ* peat surface and ground water table measurements is higher for the dry season than for the wet and whole hydrological year.

We show that the SBAS approach using C-band SAR obtains retrievals of surface displacement from 34.4 % to 59.8 % on peat soils of the tested area (391 to 826 km^2), depending on the hydrological year. Using test sites that were not subject to land cover changes (*e.g.* land clearings or fires) we showed the dependence of area effectiveness on the prevailing hydrological conditions. Whilst area-effectiveness is perhaps lower than could be achieved in less complex areas, the retrievals far exceed current *in situ* monitoring with stations only sparsely distributed across a region which is very challenging to access. The SBAS approach allows for dynamic monitoring throughout the year at 12 day temporal resolution, which is coarser than *in situ* records, but spatially-distributed. The use of the radar interferometry technique and the SBAS approach can thus significantly complement ground-based measurements, which are difficult to carry out in hard-to-reach places, as is the case in many tropical peatland areas. The dearth of readily available validation data for this study emphasises the lack of information about these factors from ground-based monitoring networks.

To assess the accuracy of the SBAS displacements, we used two types of data: peat surface and groundwater levels. Such comparisons in tropical peatlands are not known so far due to the lack of data. The studies have shown that SBAS-derived surface height values can correspond reasonably well with *in situ* surface height measurements, although the degree of agreement may vary depending on site-specific conditions, *e.g.* during the dry periods. SBAS surface height measurements showed a more complex relationship to groundwater levels, with good correspondence in some areas. Observations from a set of *in situ* monitoring stations showed however the strong correspondence between peat surface height and hydrological conditions. This reflects wider understanding of peatland hydrological dynamics where hydrological status/behaviour has a topographic signature. We note that the

verification of surface height and GWL was performed on a small number of validation points. Doing so across a larger validation area would be favourable but likely highly challenging owing to the complex spatial dynamics, land use and access within these tropical peatland areas.

We also demonstrated through examples that appropriate hydrological conditions must be met to determine the change in the water level above the ground surface. Too large fluctuations in the water level may not be detected because of wavelength limitations, and outliers from the assumed linear model may be filtered out or removed due to the used approach.

Using the short stack approach additionally demonstrates the capabilities of the SBAS approach in tropical peatlands without the need for time-consuming data collection and subsequent processing, which is beneficial for rapid operational applications. However, the displacement model should be carefully chosen as various models can bring different trend of displacements and accuracies compared to ground validation data.

CRediT authorship contribution statement

Magdalena M. Mleczko: Writing – review & editing, Writing – original draft, Visualization, Validation, Resources, Methodology, Investigation, Formal analysis, Data curation, Conceptualization. **Kitso Kusin:** Writing – original draft, Resources, Data curation. **Teuntje P. Hollaar:** Writing – review & editing, Visualization. **Mark E. Harrison:** Writing – review & editing. **Nomeritae Nomeritae:** Writing – review & editing, Resources, Data curation. **Darmae Nasir:** Writing – review & editing, Resources. **Marek S. Mróz:** Writing – review & editing, Methodology. **F.J. Frank van Veen:** Writing – review & editing, Conceptualization. **Muhammad A. Imron:** Writing – review & editing. **A. Jonay Jovani-Sancho:** Writing – review & editing, Resources, Data curation. **Chris D. Evans:** Resources. **Adi Jaya:** Writing – review & editing, Resources. **Karen Anderson:** Writing – review & editing, Writing – original draft, Supervision, Methodology, Investigation, Conceptualization.

Declaration of competing interest

The authors declare that they have no known competing financial interests or personal relationships that could have appeared to influence the work reported in this paper.

Acknowledgements

This research is funded by UK Research and Innovation (UKRI) through the Global Challenges Research Fund (GCRF) grant number NE/T010401/1.

The authors would like to thank the Indonesian National Research & Innovation Agency (BRIN) for permission to conduct research in Indonesia.

In addition, we would like to thank the Ministry of Environment and Forestry (Kementerian Lingkungan Hidup dan Kehutanan (KLHK)) for the provision of the land cover maps for our study sites.

Contains modified Copernicus Sentinel data [2015-2022].

The groundwater level data used for this work were obtained from the project PASSES: Peatland Assessment in Southeast Asia by Satellite, funded by the United Kingdom Space Agency International Partnership Program and the project SUSTAINPEAT: Overcoming barriers to sustainable livelihoods and environments in smallholder agricultural systems on tropical peatland, funded by United Kingdom Research and Innovation *via* the Global Challenges Research Fund and the Biotechnology and Biological Sciences Research Council (BBSRC) Grant number BB/P023533/1.

Appendix A. Supplementary data

Supplementary data to this article can be found online at https://doi.org/10.1016/j.rse.2025.115009.

Data availability

Data will be made available on request.

References

Alshammari, L., Large, D.J., Boyd, D.S., Sowter, A., Anderson, R., Andersen, R., Marsh, S., 2018. Long-term peatland condition assessment via surface motion monitoring using the ISBAS DInSAR technique over the flow country, Scotland. Remote Sens (Basel) 10. https://doi.org/10.3390/rs10071103.

Asmuß, T., Bechtold, M., Tiemeyer, B., 2019. On the potential of Sentinel-1 for high resolution monitoring of water table dynamics in grasslands on organic soils. Remote Sens (Basel) 11. https://doi.org/10.3390/rs11141659.

Atwood, E.C., Englhart, S., Lorenz, E., Halle, W., Wiedemann, W., Siegert, F., 2016. Detection and characterization of low temperature peat fires during the 2015 fire catastrophe in Indonesia using a new high-sensitivity fire monitoring satellite sensor (FireBird). PLoS One 11. https://doi.org/10.1371/journal.pone.0159410.

Barrett, B.W., Dwyer, E., Whelan, P., 2009. Soil moisture retrieval from active spaceborne microwave observations: an evaluation of current techniques. Remote Sens (Basel) 1. https://doi.org/10.3390/rs1030210.

Bechtold, M., Schlaffer, S., Tiemeyer, B., de Lannoy, G., 2018. Inferring water table depth dynamics from ENVISAT-ASAR C-band backscatter over a range of peatlands from deeply-drained to natural conditions. Remote Sens (Basel) 10. https://doi.org/10.3390/rs10040536.

Berardino, P., Fornaro, G., Lanari, R., Sansosti, E., 2002. A new algorithm for surface deformation monitoring based on small baseline differential SAR interferograms. IEEE Trans. Geosci. Remote Sens. 40. https://doi.org/10.1109/TGRS.2002.803792.

Brisco, B., Ahern, F., Murnaghan, K., White, L., Canisus, F., Lancaster, P., 2017. Seasonal change in wetland coherence as an aid to wetland monitoring. Remote Sens (Basel) 9, 1–19. https://doi.org/10.3390/rs9020158.

Brisco, B., Shelat, Y., Murnaghan, K., Montgomery, J., Fuss, C., Olthof, I., Hopkinson, C., Deschamps, A., Poncos, V., 2019. Evaluation of C-band SAR for identification of flooded vegetation in emergency response products. Can. J. Remote. Sens. 45, 73–87. https://doi.org/10.1080/07038992.2019.1612236.

Cai, W., Borlace, S., Lengaigne, M., Van Rensch, P., Collins, M., Vecchi, G., Timmermann, A., Santoso, A., Mcphaden, M.J., Wu, L., England, M.H., Wang, G., Guilyardi, E., Jin, F.F., 2014. Increasing frequency of extreme El Niño events due to greenhouse warming. Nat. Clim. Chang. 4. https://doi.org/10.1038/nclimate2100.

Cigna, F., Sowter, A., 2017. The relationship between intermittent coherence and precision of ISBAS InSAR ground motion velocities: ERS-1/2 case studies in the UK. Remote Sens. Environ. 202. https://doi.org/10.1016/j.rse.2017.05.016.

Crosetto, M., Monserrat, O., Cuevas-González, M., Devanthéry, N., Crippa, B., 2016. Persistent scatterer interferometry: a review. ISPRS J. Photogramm. Remote Sens. https://doi.org/10.1016/j.isprsjprs.2015.10.011.

Dabrowska-Zielinska, K., Musial, J., Malinska, A., Budzynska, M., Gurdak, R., Kiryla, W., Bartold, M., Grzybowski, P., 2018. Soil moisture in the Biebrza wetlands retrieved from Sentinel-1 imagery. Remote Sens (Basel) 10. https://doi.org/10.3390/rs10121979.

Davies-Barnard, T., Catto, J.L., Harper, A.B., Imron, M.A., Frank van Veen, F.J., 2023. Future fire risk under climate change and deforestation scenarios in tropical Borneo. Environ. Res. Lett. 18. https://doi.org/10.1088/1748-9326/acb225.

de Zan, F., Parizzi, A., Prats-Iraola, P., López-Dekker, P., 2014. A SAR interferometric model for soil moisture. IEEE Trans. Geosci. Remote Sens. 52. https://doi.org/10.1109/TGRS.2013.2241069.

Dellepiane, S.G., Angiati, E., 2012. A new method for cross-normalization and multitemporal visualization of SAR images for the detection of flooded areas. IEEE Trans. Geosci. Remote Sens. 50, 2765–2779. https://doi.org/10.1109/TGRS.2011.2174999.

Devanthéry, N., Crosetto, M., Monserrat, O., Cuevas-González, M., Crippa, B., 2014. An approach to persistent scatterer interferometry. Remote Sens (Basel) 6. https://doi.org/10.3390/rs6076662.

Doin, M.P., Lasserre, C., Peltzer, G., Cavalié, O., Doubre, C., 2009. Corrections of stratified tropospheric delays in SAR interferometry: validation with global atmospheric models. J. Appl. Geophys. 69. https://doi.org/10.1016/j.jappgeo.2009.03.010.

ESA, 2019. Copernicus DEM - Global and European Digital Elevation Model [WWW Document]. URL. https://dataspace.copernicus.eu/explore-data/data-collections/copernicus-contributing-missions/collections-description/COP-DEM (accessed 2.16.25).

Evans, C.D., Callaghan, N., Jaya, A., Grinham, A., Sjogersten, S., Page, S.E., Harrison, M. E., Kusin, K., Kho, L.K., Ledger, M., Evers, S., Mitchell, Z., Williamson, J., Radbourne, A.D., Jovani-Sancho, A.J., 2021. A novel low-cost, high-resolution camera system for measuring peat subsidence and water table dynamics. Front. Environ. Sci. 9. https://doi.org/10.3389/fenvs.2021.630752.

Goldstein, R.M., Werner, C.L., 1998. Radar interferogram filtering for geophysical applications. Geophys. Res. Lett. 25. https://doi.org/10.1029/1998GL900033.

Gondwe, B.R.N., Hong, S.-H., Wdowinski, S., Bauer-Gottwein, P., 2010. Hydrologic dynamics of the ground-water-dependent Sian ka'an wetlands, Mexico, derived from

InSAR and SAR data. Wetlands 30, 1–13. https://doi.org/10.1007/s13157-009-0016-z.
Greifeneder, F., Notarnicola, C., Wagner, W., 2021. A machine learning-based approach for surface soil moisture estimations with google earth engine. Remote Sens (Basel) 13. https://doi.org/10.3390/rs13112099.
Grimaldi, S., Xu, J., Li, Y., Pauwels, V.R.N., Walker, J.P., 2020. Flood mapping under vegetation using single SAR acquisitions. Remote Sens. Environ. 237. https://doi.org/10.1016/j.rse.2019.111582.
Hanssen, R.F., 2001. Radar interferometry - data interpretation and error analysis. J. Phys. A Math. Theor. https://doi.org/10.1007/0-306-47633-9.
Hayasaka, H., Usup, A., Naito, D., 2020. New approach evaluating peatland fires in Indonesian factors. Remote Sens (Basel) 12. https://doi.org/10.3390/RS12122055.
He, Y., Zhang, G., Kaufmann, H., Xu, G., 2021. Automatic interferogram selection for SBAS-InSAR based on deep convolutional neural networks. Remote Sens (Basel) 13, 4468. https://doi.org/10.3390/rs13214468.
Hong, S.H., Wdowinski, S., 2014. Multitemporal multitrack monitoring of wetland water levels in the florida everglades using alos palsar data with interferometric processing. IEEE Geosci. Remote Sens. Lett. 11. https://doi.org/10.1109/LGRS.2013.2293492.
Hong, S.H., Wdowinski, S., Kim, S.W., 2022. Extraction of absolute water level using TanDEM-X bistatic observations with a Large perpendicular baseline. IEEE Geosci. Remote Sens. Lett. 19. https://doi.org/10.1109/LGRS.2021.3086875.
Hoscilo, A., Page, S.E., Tansey, K.J., Rieley, J.O., 2011. Effect of repeated fires on land-cover change on peatland in southern Central Kalimantan, Indonesia, from 1973 to 2005. Int. J. Wildland Fire 20. https://doi.org/10.1071/WF10029.
Hoyt, A.M., Chaussard, E., Seppalainen, S.S., Harvey, C.F., 2024. Quantifying Subsidence in Tropical Peatlands, pp. 347–357 doi: 10.1007/978-3-031-59306-2_16.
Hoyt, A.M., Chaussard, E., Seppalainen, S.S., Harvey, C.F., 2020. Widespread subsidence and carbon emissions across southeast Asian peatlands. Nat. Geosci. 13. https://doi.org/10.1038/s41561-020-0575-4.
Hrysiewicz, A., Holohan, E.P., Donohue, S., Cushnan, H., 2023. SAR and InSAR data linked to soil moisture changes on a temperate raised peatland subjected to a wildfire. Remote Sens. Environ. 291, 113516. https://doi.org/10.1016/j.rse.2023.113516.
Hrysiewicz, A., Williamson, J., Evans, C.D., Jovani-Sancho, A.J., Callaghan, N., Lyons, J., White, J., Kowalska, J., Menichino, N., Holohan, E.P., 2024. Estimation and validation of InSAR-derived surface displacements at temperate raised peatlands. Remote Sens. Environ. 311, 114232. https://doi.org/10.1016/J.RSE.2024.114232.
Izumi, Y., Takeuchi, W., Widodo, J., Sulaiman, A., Awaluddin, A., Aditiya, A., Razi, P., Anggono, T., Sri Sumantyo, J.T., 2022a. A 3-year tropical peatland subsidence time-series derived by sentinel- 1: a case study of the Kalimantan, Indonesia. In: IGARSS 2022–2022 IEEE International Geoscience and Remote Sensing Symposium, pp. 7863–7866. https://doi.org/10.1109/IGARSS46834.2022.9883791.
Izumi, Y., Takeuchi, W., Widodo, J., Sulaiman, A., Awaluddin, A., Aditiya, A., Razi, P., Anggono, T., Sumantyo, J.T.S., 2022b. Temporal subset SBAS InSAR approach for tropical peatland surface deformation monitoring using Sentinel-1 data. Remote Sens (Basel) 14. https://doi.org/10.3390/rs14225825.
Khakim, M.Y.N., Bama, A.A., Yustian, I., Poerwono, P., Tsuji, T., Matsuoka, T., 2020. Peatland subsidence and vegetation cover degradation as impacts of the 2015 El niño event revealed by sentinel-1A SAR data. Int. J. Appl. Earth Obs. Geoinf. 84. https://doi.org/10.1016/j.jag.2019.101953.
Kim, J.W., Lu, Z., Gutenberg, L., Zhu, Z., 2017. Characterizing hydrologic changes of the great dismal swamp using SAR/InSAR. Remote Sens. Environ. 198. https://doi.org/10.1016/j.rse.2017.06.009.
KLHK, 2022. Geospatial data of land cover and soils in Indonesia 2017-2022 provided by the Ministry of Environment and Forestry Indonesia (KLHK) [Database]. URL (accessed 2.15.25). https://sigap.menlhk.go.id.
Kusin, K., Kusin, K., Jagau, Y., Ricardo, J., Saman, T.N., Aguswan, Y., Aguswan, Y., 2020. Peat lost by fire in Kalampangan area, Central Kalimantan, Indonesia. In: IOP Conference Series: Earth and Environmental Science. https://doi.org/10.1088/1755-1315/504/1/012009.
Ledger, M.J., Evans, C.D., Large, D.J., Evers, S., Brown, C., Jovani-Sancho, A.J., Callaghan, N., Vane, C.H., Marshall, C., Baskaran, A., Gan, J.Y., Sowter, A., Morrison, K., Sjögersten, S., 2023. Tropical peat surface oscillations are a function of peat condition at North Selangor peat swamp forest, Malaysia. Front. Environ. Sci. 11. https://doi.org/10.3389/fenvs.2023.1182100.
Li, S., Xu, W., Li, Z., 2022. Review of the SBAS InSAR time-series algorithms, applications, and challenges. Geod. Geodyn. 13. https://doi.org/10.1016/j.geog.2021.09.007.
Liao, H., Wdowinski, S., Li, S., 2020. Regional-scale hydrological monitoring of wetlands with Sentinel-1 InSAR observations: case study of the South Florida Everglades. Remote Sens. Environ. 251. https://doi.org/10.1016/j.rse.2020.112051.
Liu, J., Bowman, K.W., Schimel, D.S., Parazoo, N.C., Jiang, Z., Lee, M., Bloom, A.A., Wunch, D., Frankenberg, C., Sun, Y., O'Dell, C.W., Gurney, K.R., Menemenlis, D., Gierach, M., Crisp, D., Eldering, A., 2017. Contrasting carbon cycle responses of the tropical continents to the 2015–2016 El Niño. Science 1979, 358. https://doi.org/10.1126/science.aam5690.
Lopez-Sanchez, J.M., Ballester-Berman, J.D., Vicente-Guijalba, F., Cloude, S.R., McNairn, H., Shang, J., Skriver, H., Jagdhuber, T., Hajnsek, I., Pottier, E., Marechal, C., Hubert-Moy, L., Corgne, S., Wdowinski, S., Touzi, R., Gosselin, G., Brooks, R., Yamaguchi, Y., Singh, G., 2021. Agriculture and Wetland Applications, pp. 119–178. https://doi.org/10.1007/978-3-030-56504-6_3.
Marshall, C., Large, D.J., Athab, A., Evers, S.L., Sowter, A., Marsh, S., Sjögersten, S., 2018. Monitoring tropical peat related settlement using ISBAS InSAR, Kuala Lumpur international airport (KLIA). Eng. Geol. 244. https://doi.org/10.1016/j.enggeo.2018.07.015.
Marshall, C., Sterk, H.P., Gilbert, P.J., Andersen, R., Bradley, A.V., Sowter, A., Marsh, S., Large, D.J., 2022. Multiscale variability and the comparison of ground and satellite radar based measures of peatland surface motion for peatland monitoring. Remote Sens (Basel) 14. https://doi.org/10.3390/rs14020336.
Matgen, P., Hostache, R., Schumann, G., Pfister, L., Hoffmann, L., Savenije, H.H.G., 2011. Towards an automated SAR-based flood monitoring system: lessons learned from two case studies. Phys. Chem. Earth 36. https://doi.org/10.1016/j.pce.2010.12.009.
McAlpine, C.A., Johnson, A., Salazar, A., Syktus, J., Wilson, K., Meijaard, E., Seabrook, L., Dargusch, P., Nordin, H., Sheil, D., 2018. Forest loss and Borneo's climate. Environ. Res. Lett. 13. https://doi.org/10.1088/1748-9326/aaa4ff.
Minasny, B., Berglund, Ö., Connolly, J., Hedley, C., de Vries, F., Gimona, A., Kempen, B., Kidd, D., Lilja, H., Malone, B., McBratney, A., Roudier, P., O'Rourke, S., Rudiyanto Padarian, J., Poggio, L., ten Caten, A., Thompson, D., Tuve, C., Widyatmanti, W., 2019. Digital mapping of peatlands – a critical review. Earth Sci. Rev. https://doi.org/10.1016/j.earscirev.2019.05.014.
Mleczko, M., Mroz, M., Fitrzyk, M., 2021. Riparian wetland mapping and inundation monitoring using amplitude and bistatic coherence data from the TanDEM-X Mission. IEEE J. Sel. Top Appl. Earth Obs. Remote Sens. https://doi.org/10.1109/JSTARS.2021.3054994.
Molan, Y.E., Lu, Z., 2020. Modeling InSAR phase and SAR intensity changes induced by soil moisture. IEEE Trans. Geosci. Remote Sens. 58, 4967–4975. https://doi.org/10.1109/TGRS.2020.2970841.
Mora, O., Mallorqui, J.J., Broquetas, A., 2003. Linear and nonlinear terrain deformation maps from a reduced set of interferometric SAR images. IEEE Trans. Geosci. Remote Sens. 41. https://doi.org/10.1109/TGRS.2003.814657.
Page, S., Hosciło, A., Wösten, H., Jauhiainen, J., Silvius, M., Rieley, J., Ritzema, H., Tansey, K., Graham, L., Vasander, H., Limin, S., 2009. Restoration ecology of lowland tropical peatlands in Southeast Asia: current knowledge and future research directions. Ecosystems 12. https://doi.org/10.1007/s10021-008-9216-2.
Page, S.E., Rieley, J.O., Banks, C.J., 2011. Global and regional importance of the tropical peatland carbon pool. Glob. Chang. Biol. 17. https://doi.org/10.1111/j.1365-2486.2010.02279.x.
Palamà, R., Crosetto, M., Rapinski, J., Barra, A., Cuevas-González, M., Monserrat, O., Crippa, B., Kotulak, N., Mróz, M., Mleczko, M., 2022. A multi-temporal small baseline interferometry procedure applied to mining-induced deformation monitoring. Remote Sens (Basel) 14. https://doi.org/10.3390/rs14092182.
Plank, S., Jussi, M., Martinis, S., Twele, A., 2017. Combining polarimetric sentinel-1 and ALOS-2/PALSAR-2 imagery for mapping of flooded vegetation. In: International Geoscience and Remote Sensing Symposium (IGARSS). IEEE, pp. 5705–5708. https://doi.org/10.1109/IGARSS.2017.8128303.
Posa, M.R.C., Wijedasa, L.S., Corlett, R.T., 2011. Biodiversity and conservation of tropical peat swamp forests. Bioscience 61. https://doi.org/10.1525/bio.2011.61.1.10.
Price, J.S., McCarter, C.P.R., Quinton, W.L., 2023. Groundwater in peat and peatlands. The Groundwater Project. https://doi.org/10.21083/978-1-77470-015-0.
Pulvirenti, L., Chini, M., Pierdicca, N., Boni, G., 2016. Use of SAR data for detecting floodwater in urban and agricultural areas: the role of the interferometric coherence. IEEE Trans. Geosci. Remote Sens. https://doi.org/10.1109/TGRS.2015.2482001.
Putra, E.I., 2011. The effect of the precipitation pattern of the dry season on peat fire occurrence in the mega Rice project area, Central Kalimantan, Indonesia. Tropics 19. https://doi.org/10.3759/tropics.19.145.
Ranjbar, S., Akhoondzadeh, M., Brisco, B., Amani, M., Hosseini, M., 2021. Soil moisture change monitoring from C and L-band SAR interferometric phase observations. IEEE J. Sel. Top. Appl. Earth Obs. Remote Sens 14. https://doi.org/10.1109/JSTARS.2021.3096063.
Ribeiro, K., Pacheco, F.S., Ferreira, J.W., de Sousa-Neto, E.R., Hastie, A., Krieger Filho, G. C., Alvalá, P.C., Forti, M.C., Ometto, J.P., 2021. Tropical peatlands and their contribution to the global carbon cycle and climate change. Glob. Chang. Biol. https://doi.org/10.1111/gcb.15408.
Sarmap, 2022. SBAS Tutorial.
Scott, C.P., Lohman, R.B., Jordan, T.E., 2017. InSAR constraints on soil moisture evolution after the march 2015 extreme precipitation event in Chile. Sci. Rep. 7. https://doi.org/10.1038/s41598-017-05123-4.
Sowter, A., Bateson, L., Strange, P., Ambrose, K., Fifiksyafiudin, M., 2013. Dinsar estimation of land motion using intermittent coherence with application to the south derbyshire and leicestershire coalfields. Remote Sens. Lett. 4. https://doi.org/10.1080/2150704X.2013.823673.
Sze, J.S., Jefferson Lee, J.S.H., 2019. Evaluating the social and environmental factors behind the 2015 extreme fire event in Sumatra, Indonesia. Environ. Res. Lett. 14. https://doi.org/10.1088/1748-9326/aaee1d.
Tampuu, T., Praks, J., Kull, A., 2020a. Insar coherence for monitoring water table fluctuations in Northern Peatlands. In: International Geoscience and Remote Sensing Symposium (IGARSS). https://doi.org/10.1109/IGARSS39084.2020.9323709.
Tampuu, T., Praks, J., Uiboupin, R., Kull, A., 2020b. Long term interferometric temporal coherence and DInSAR phase in northern peatlands. Remote Sens (Basel) 12. https://doi.org/10.3390/rs12101566.
Tampuu, T., De Zan, F., Shau, R., Praks, J., Kohv, M., Kull, A., 2022. Can bog breathing be measured by Synthetic Aperture Radar Interferometry. In: IGARSS 2022–2022 IEEE International Geoscience and Remote Sensing Symposium, pp. 16–19. https://doi.org/10.1109/IGARSS46834.2022.9883421.
Tampuu, T., Praks, J., De Zan, F., Kohv, M., Kull, A., 2023. Relationship between ground levelling measurements and radar satellite interferometric estimates of bog breathing in ombrotrophic northern bogs. Mires Peat 29. https://doi.org/10.19189/MaP.2022.OMB.Sc.1999815.
Tanase, M.A., Belenguer-Plomer, M.A., Roteta, E., Bastarrika, A., Wheeler, J., Fernández-Carrillo, Á., Tansey, K., Wiedemann, W., Navratil, P., Lohberger, S., Siegert, F.,

Chuvieco, E., 2020. Burned area detection and mapping: intercomparison of Sentinel-1 and Sentinel-2 based algorithms over tropical Africa. Remote Sens (Basel) 12. https://doi.org/10.3390/rs12020334.
Thirumalai, K., DInezio, P.N., Okumura, Y., Deser, C., 2017. Extreme temperatures in Southeast Asia caused by El Ninō and worsened by global warming. Nat. Commun. 8. https://doi.org/10.1038/ncomms15531.
Torres, R., Lokas, S., Di Cosimo, G., Geudtner, D., Bibby, D., 2017. Sentinel 1 Evolution: Sentinel-1C and -1D Models, in: International Geoscience and Remote Sensing Symposium (IGARSS). https://doi.org/10.1109/IGARSS.2017.8128261.
Tsyganskaya, V., Martinis, S., Marzahn, P., Ludwig, R., 2018. Detection of temporary flooded vegetation using Sentinel-1 time series data. Remote Sens (Basel) 10, 1286. https://doi.org/10.3390/rs10081286.
Umarhadi, D.A., Avtar, R., Widyatmanti, W., Johnson, B.A., Yunus, A.P., Khedher, K.M., Singh, G., 2021. Use of multifrequency (C-band and L-band) SAR data to monitor peat subsidence based on time-series SBAS InSAR technique. Land Degrad. Dev. 32. https://doi.org/10.1002/ldr.4061.
Umarhadi, D.A., Avtar, R., Kumar, P., Yunus, A.P., Kurniawan, T.A., Kharrazi, A., Ishikawa, M., Widyatmanti, W., 2022. Monitoring tropical peatlands subsidence by time-series interferometric synthetic aperture radar (InSAR) technique. In: Radar Remote Sensing: Applications and Challenges. https://doi.org/10.1016/B978-0-12-823457-0.00013-6.
Waqar, M.M., Sukmawati, R., Ji, Y., Sri Sumantyo, J.T., 2020. Tropical peatland forest biomass estimation using polarimetric parameters extracted from RadarSAT-2 images. Land (Basel) 9. https://doi.org/10.3390/LAND9060193.
Widodo, J., Izumi, Y., Takahashi, A., Kausarian, H., Perissin, D., Sri Sumantyo, J.T., 2019. Detection of peat fire risk area based on impedance model and DInSAR approaches using ALOS-2 PALSAR-2 data. IEEE Access 7. https://doi.org/10.1109/ACCESS.2019.2899080.
Widyatmanti, W., Minasny, B., Awanda, D., Umarhadi, D.A., Fatma, Z.S.N., Mahendra, W.K., Field, D.J., 2022. Codification to secure Indonesian peatlands: from policy to practices as revealed by remote sensing analysis. Soil Security 9, 100080. https://doi.org/10.1016/j.soisec.2022.100080.
World Bank Group, 2018. Pilot Ecosystem Account for Indonesian Peatlands.
World Bank Group, Asian Development Bank, 2021. Climate Risk Country Profile INDONESIA.
Wösten, J.H.M., Ismail, A.B., van Wijk, A.L.M., 1997. Peat subsidence and its practical implications: a case study in Malaysia. Geoderma 78. https://doi.org/10.1016/S0016-7061(97)00013-X.
Wösten, J.H.M., Clymans, E., Page, S.E., Rieley, J.O., Limin, S.H., 2008. Peat-water interrelationships in a tropical peatland ecosystem in Southeast Asia. Catena (Amst.) 73. https://doi.org/10.1016/j.catena.2007.07.010.
Yunjun, Z., Fattahi, H., Amelung, F., 2019. Small baseline InSAR time series analysis: unwrapping error correction and noise reduction. Comput. Geosci. https://doi.org/10.1016/j.cageo.2019.104331.
Zhang, Y., Liu, Yaolin, Jin, M., Jing, Y., Liu, Yi, Liu, Yanfang, Sun, W., Wei, J., Chen, Y., 2019. Monitoring land subsidence in Wuhan city (China) using the SBAS-INSAR method with radarsat-2 imagery data. Sensors (Switzerland) 19. https://doi.org/10.3390/s19030743.
Zheng, X., Wang, C., Tang, Y., Zhang, H., Li, T., Zou, L., Guan, S., 2023. Adaptive high coherence temporal subsets SBAS-InSAR in tropical peatlands degradation monitoring. Remote Sens (Basel) 15. https://doi.org/10.3390/rs15184461.
Zhou, Z., Li, Z., Waldron, S., Tanaka, A., 2019. InSAR time series analysis of L-band data for understanding tropical peatland degradation and restoration. Remote Sens (Basel) 11. https://doi.org/10.3390/rs11212592.
Zwieback, S., Hensley, S., Hajnsek, I., 2015. Assessment of soil moisture effects on L-band radar interferometry. Remote Sens. Environ. 164. https://doi.org/10.1016/j.rse.2015.04.012.
Zwieback, S., Hensley, S., Hajnsek, I., 2017. Soil moisture estimation using differential radar interferometry: toward separating soil moisture and displacements. IEEE Trans. Geosci. Remote Sens. 55. https://doi.org/10.1109/TGRS.2017.2702099.